Project funded by the European Commission under the 6th (EC) RTD Framework Programme (2002- 2006) within the framework of the specific research and technological development programme "Integrating and strengthening the European Research Area"

Project UpWind

Contract No.:

019945 (SES6)

"Integrated Wind Turbine Design"

ADAPTIVE WIND TURBINE BLADE BASED ON SMA COMPOSITES

D1B3.11: A representative part of a blade, which shows the construction, the robustness and the physical realization of the sensors and actuators

AUTHOR:	Tomi Lindroos
AFFILIATION:	VTT Technical Research Centre of Finland
ADDRESS:	Sinitaival 6 33101 Tampere Finland
TEL.:	+358 503020227
EMAIL:	tomi.lindroos@vtt.fi
FURTHER AUTHORS:	
REVIEWER:	Project members
APPROVER:	

Document Information

DOCUMENT TYPE	Deliverable
Document Name:	ADAPTIVE WIND TURBINE BLADE BASED ON SMA COMPOSITES
REVISION:	
REV.DATE:	
CLASSIFICATION:	R1: Restricted to project members
STATUS:	

Contents

1. Introduction 5
PART I: Adaptive blade based on conventional SMA composites 6
2. SMA composites 6
2.1 Designing of structure 6
2.2 Manufacturing of test structure 8
2.3 Testing 12
2.4 Wind Tunnel Tests 13
2.5 Conclusions 17
PART II: Adaptive modular blade based on R-phase transformation 18
3. R-phase transformation 18
4. Modelling 18
4.1 Heat transfer modelling 18
4.2 Conclusion 23
4.3 Modelling of NiTi SMA wire actuators 24
4.4 Modelling of a R-phase actuated trailing edge 25
5. Pressure sensors for detection disturbance in airflow 30
5.1 Test setup and measurements 30
6. Designing and manufacturing of modular structure 34
7. R-phase actuated adaptive composites 35
7.1 Manufacturing R-phase composites 35
7.2 Manufacturing of prototype for wind tunnel measurement 37
8. Testing 38
8.1 Preliminary tests 38
8.2 Wind tunnel tests 40
9. Conclusions 45
10. References 46

STATUS, CONFIDENTIALITY AND ACCESSIBILITY								
Status				**Confidentiality**			**Accessibility**	
S0	Approved/Released			**R0**	General public		Private web site	x
S1	Reviewed	**x**		**R1**	Restricted to project members	x	Public web site	
S2	Pending for review			**R2**	Restricted to European. Commission		Paper copy	
S3	Draft for commends			**R3**	Restricted to WP members + PL			
S4	Under preparation			**R4**	Restricted to Task members +WPL+PL			

PL: *Project leader* **WPL:** *Work package leader* **TL:** *Task leader*

ADAPTIVE WIND TURBINE BLADE BASED ON SMA COMPOSITES

1. Introduction

There is an interest of doubling or quadrupling the rated power of wind turbines from the present maximum of about 5 MW, especially for offshore applications. This increases the blade length to about 80 or 100 m. The growth in size of blades is not feasible using the present technologies and materials. Also the slenderness of wind turbines is leading to increased importance of vibration and fatigue control of blades and supporting structures. These increasing requirements call for new structural concepts and advanced materials and also for more adaptive solutions.

Better control of the turbine such as advanced blade pitch control, advanced generator control and airfoil shape control or their combination has to be developed and utilized. In wind turbines the most promising concept is reduction of the fatigue loads, which can be used to increase the life of the structure or to enable use of the turbine at higher wind speeds and gusty winds, which would increase the power production [i].

Adaptive and active structures have been shown to have a great potential for creating new solutions for industrial products and processes.

The aim of this research work is to design and manufacture real scale representative part of wind turbine blade with adaptive trailing edge for wind tunnel test.

Lightweight and effectively load bearing shell structure is a common structural element in many vehicles, machines and devices. Fibre Reinforced Plastic (FRP) composite and sandwich structures are particularly interesting from the viewpoint of smart structures because their mechanical properties are relatively easy to tailor (fibre orientation, stacking of fibre layers, asymmetry etc.).

PART I: Adaptive blade based on conventional SMA composites

2. SMA composites

In different approaches, shape memory materials have usually been integrated within monolithic or composite host materials to produce the desired components where functionality or static and dynamic properties could be enhanced or actively tuned in response to environmental changes. Partly because of technically less challenging practical manufacturing processes, most of the efforts with embedded shape memory fibre containing composites have been directed to thermoplastic and thermoset polymer matrix composites [[ii], [iii]].

Generally, the shape memory composites can be manufactured with conventional fibre reinforced polymer composite fabrication methods. Many modifications concerning the basic manufacturing process have been presented in the literature [[iv],[v],[vi]].

Polymer composites with embedded shape memory materials have been demonstrated in shape and position control, active and passive control of vibration and acoustic transmission of creep resistant materials subjected to dynamic loads, or impact damage in structures.

In an active airfoil the aim is to control the shape of the airfoil to control the drag and lift properties [[vii]]. This can then be used for many applications, for example in a transonic aeroplane shape control it can be used to reduce drag and thus to reduce fuel consumption [[viii]].

However, the studies of SMA based functional composites have revealed the lack of basic knowledge in understanding the SMA material behaviour. Especially the issues concerning the generation of recovery stresses of embedded SMA wires are found to be very important. Designing and manufacturing of complicated structures requires extensive knowledge on the thermo-mechanical behaviour of the adaptive composites. Despite of this, only a few studies have been presented [[ix],[x],[xi]]. The task is very challenging where the complex thermo-mechanical behaviour of Ni-Ti interacting with the matrix material should be taken account.

2.1 Designing of structure

The aim of this study is to develop more advanced designs and manufacturing tools to produce adaptive airfoils in real scale. Furthermore, the aim is to study what is possible to replace as a part of the wind turbine blade.

Usually NiTi wires are pre-strained before embedding to the composite. The pre-straining happens by orientation of the randomly oriented martensitic variants. Depending of strain level some fraction of the structure consists of preferentially oriented

martensite and randomly oriented so called self-accommodated martensite. After prestaining, the wires are laminated inside the matrix and the composite is cured.

Activation of the SMA wires causes several simultaneous developments. When the activation temperature exceeds phase transformation temperature, the martensite phase starts to transform to the austenite. At same time stress level in the wire increases. If the stress level increases higher than stress needed to orient the remaining randomly oriented self-accommodated martensite, a re-orientation could happen simultaneously than preferentially oriented martensite phase transforms to austenite. Because of this, for example modelling of recovery stress generation has been found as a very challenging task. In most of studies modelling is used only indicative tool.

Furthermore, when the stress in the SMA exceeds the plateau stress, it also shifts the phase transformation temperatures upwards, which means that the wires need to be heated up to higher than “nominal” transformation temperature to produce full phase transformation. In many experiments reported in literature this shift of transformation temperatures has not been taken into account and therefore the heating has been inadequate. In such cases in embedded SMA wires, only a small part of the potential transformation takes place. This means that the pre-strain of the wires does not have a straight effect on the generation of recovery stresses. Increasing the heating gives more transformation, but at a slow rate.

The manufacturing process of adaptive SMA composites has only a few differences to traditional manufacturing of FRP composites. The most challenging procedure is the embedding of the SMA wires into the structure. Integration of the SMA wires is always some kind of a compromise between maximum force generation and structural integrity. By using large diameter wires it is possible to generate high force-to-volume ratio, but this may increase local stress concentrations and lead to cracking and delamination of the composite structure. Typical manufacturing process of SMA composites includes an assembly jig where SMA wires are stretched and reinforcement layers are laminated around the SMA wires. This type of manufacturing procedure is very sensitive to surface treatments of the SMA wires and de-bonding of the wires can easily happens. From the industrial manufacturing point of view, this procedure is quite impractical.

Memory-Metalle alloy M SMA wire with diameter of 0.49 mm was selected as actuator wire. In the first stage, the behaviour of the wire was exactly determined. Effect of applied stress on transformation temperatures was determined by Dynamic Mechanical Thermal Analysis (DMTA) Classius-Claperon constant were determined from hysteresis curves.

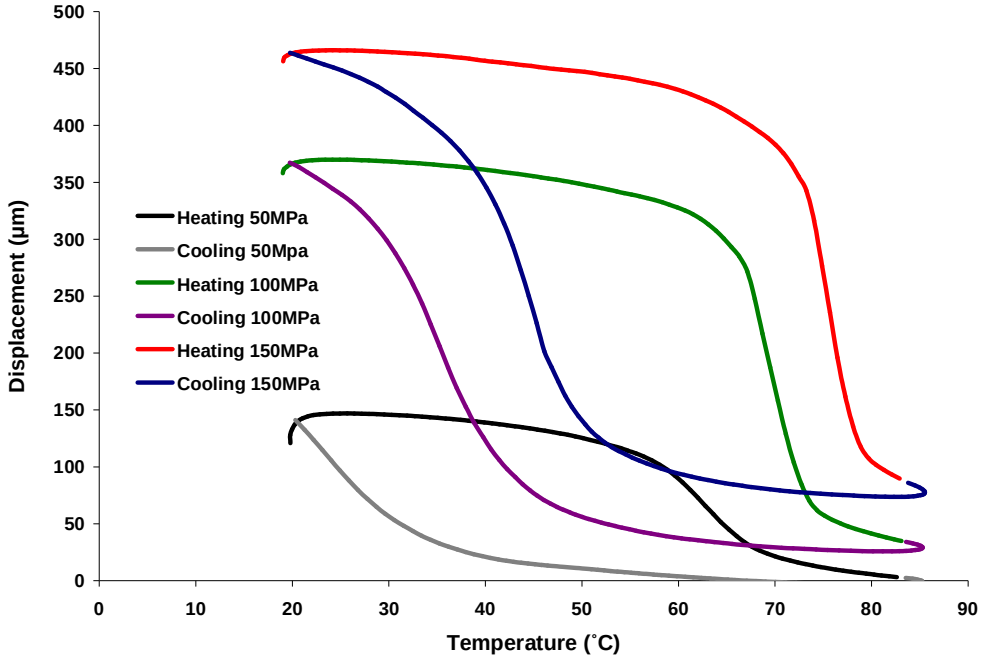

Fig. 1. Effect of applied stress on transformation behaviour of Memory-Metalle alloy M SMA wire.

Table 1. Effect of applied stress on transformation temperatures

	Classius-Clapeyron coeffi-cinets (MPa/˚C)
As	5,9
Af	10,1
Ms	4,8
Mf	4,0

2.2 Manufacturing of test structure

NACA 63-215 airfoil representing typical wind turbine blade cross-section was chosen as the test platform structure. Dimensions of the airfoil were chosen so that it equals a typical blade section dimensions taken approximately 5m from the tip of the blade (chord 700 mm). The real situation was simplified by using constant cross-section across airfoil length.

Gurit Prime 20 LV slow hardener epoxy systems was chosen as matrix material. After the standard curing cycle of the composite the glass transition temperature (Tg temperature) of the epoxy matrix is located near 80 ºC. This means that the maximum temperature of the SMA wire should be restricted below that temperature. Af tempera-

ture of the SMA wire is 64 ºC without applied stress, where it means that maximum recovery stress generated by SMA wire could be 100 MPa without damaging composite. By using this knowledge, the amount of required SMA wire actuators can be estimated to achieve desired shape change with a certain composite structure.

Desired shape changes of the airfoil were determined by FE modelling. The composite structure of the adaptive airfoil were modelled by using the ABAQUS FE program both as 3D and shell models using with the rebar and rebar shell options of ABAQUS for the SMA wires. The contraction of the SMA wires was modelled by thermal expansion analogy with a negative thermal expansion coefficient. Thus the models cannot give absolute displacements nor the correct displacement history but only the relative shape of the deformed structure.

Because of the lack of adequate material model describing the SMA wires in actuator mode the development work was started by manufacturing airfoil cross-sections with only 100 mm span width. The structure of the airfoil was slightly modified after measurement so that better correspondence to modelled shape change could be achieved. After some iterative routes the shape obtained with the model corresponded well with the experimentally obtained shape [xii].Because high actuation forces are needed to deform the airfoil, the distance between neighbouring SMA wires were chosen to be about 4 mm. The stiffness of the laminate structure was determined to correspond on the other hand recovery stress generation of SMA wires, and the effect of applied external load. Fibre layout structure is presented in

Table 2 where zero axis is parallel to span length.

Table 2. Layout of reinforcing fibres

Layer	Angle	Material	Weight (g/m$^{2)}$	Distance from trailing edge Start (mm)	End (mm)
upper laminate					
U1	0/90º	E-Glass fabric	270	0	700
U2	90º	E-Glass UD	750	0	700
U3	90º	E-Glass UD	750	100	700
U4	90º	E-Glass UD	750	200	700
U5	90º	E-Glass UD	750	300	700
U7	90º	E-Glass UD	750	400	700
U8	+/-45º	Aramid fabric	170	0	400
U9	90º	SMA d 0.49 mm spacing 4 mm		50	330
U10	+/-45º	Aramid fabric	170	0	400
U11	0/90º	E-Glass fabric	270	330	700
S4		Strain gage 4		175	
S5		Strain gage 5		100	
lower laminate					
S1		Strain gage 1		180	
S2		Strain gage 2		105	
S3		Strain gage 3		160	
L1	0/90º	E-Glass UD	270	0	700
L2	0º UD	E-Glass UD	750	0	700
L3	0º UD	E-Glass UD	750	0	700
L4	0º UD	E-Glass UD	750	0	700
L5	0º UD	E-Glass UD	750	400	700
L6	+/-45º	Aramid fabric	170	0	400
L7	90º	SMA d 0.49 mm spacing 4 mm		50	330
L8	+/-45º	Aramid fabric	170	0	400
L9	0º UD	E-Glass UD	750	300	700
L10	0/90º	E-Glass fabric	270	330	700

In literature, generally two different approaches are reported to be used in manufacturing of SMA composites. In the first one the SMA wires are placed inside mechanical sleeves and in the second a more sophisticated method, an adhesive bond is created between the SMA wire and the matrix. The adhesive bond is very critical on the stress and temperature levels of the SMA wires.

In this study a more advanced method was developed to manufacture SMA composites. The method is a combination of mechanical sleeves and adhesive bonding, where the SMA wires are anchored with reinforcing aramid fibre tows. In this way the forces generated by SMA wires are mostly carried by anchoring tows instead of adhesive bond between actuator wire and matrix. The new method enables the use of larger diameter wires because the forces generated by the wires are evenly distributed and pullout of wires is prevented.

The manufacturing of an adaptive airfoil comprises of two steps: 1) Manufacturing of the insert actuator laminate which includes the SMA wires and the desired sensors. 2) Manufacturing of the actual airfoil including the insert actuator laminate.Insert laminates were manufactured in an assembly jig designed and manufactured for this purpose. The manufacturing of insert laminate was started by producing the woven-like structure, where SMA wires were connected to assembly jig by aramid tows. At this

stage electrical connections and temperature sensor were also installed. This woven-like structure was laminated between two aramid fabrics and cured before loosening of jig assembly.

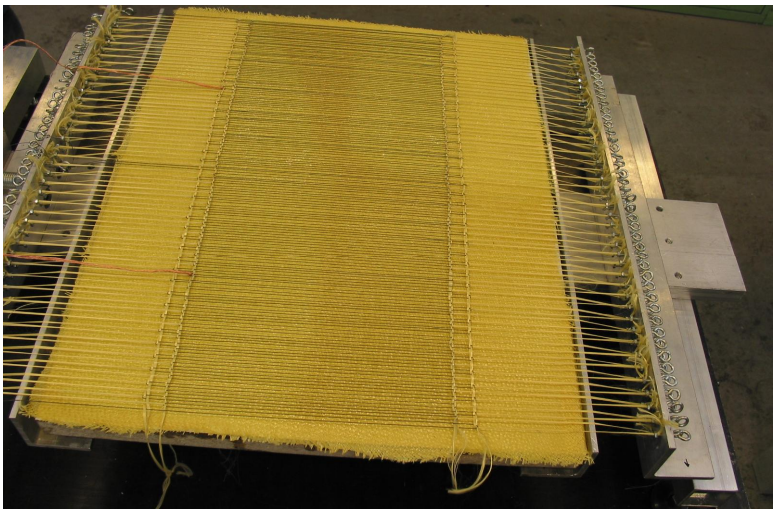

Fig. 2. Woven like structure of SMA wires and aramid tows before lamination.

Airfoil skin laminates were manufactured by vacuum infusion. Reinforcing fibre layer was assembled to mould together insert laminates.

2.3 Testing

Before wind tunnel tests, a series of functionality tests was done to the airfoil at laboratory. Functionality of sensors, actuators and control systems were determined by temperature and strain controlled activation loops. In *Fig. 3* shape change of the airfoil is shown at different temperatures. The difference of trailing edge angle between room temperature (RT) and maximum activation temperature 65°C is approximately 6°.

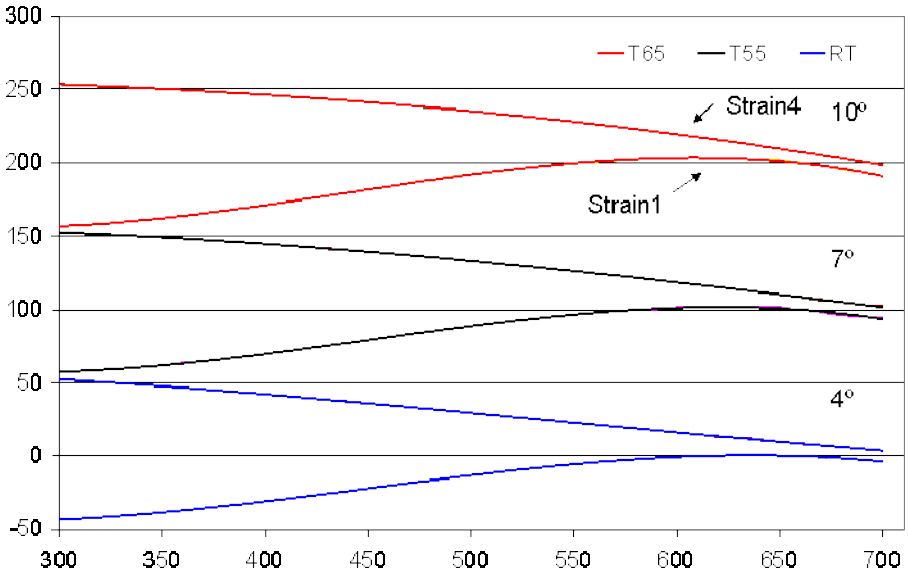

Fig. 3. Shape change of airfoil at different temperatures in laboratory measurements.

2.4 Wind Tunnel Tests

The airfoil section of a wind turbine blade with one meter span was installed and tested in a low speed wind tunnel to find aerodynamic properties of the shape controlled airfoil. The test setup is shown in *Fig. 4*.

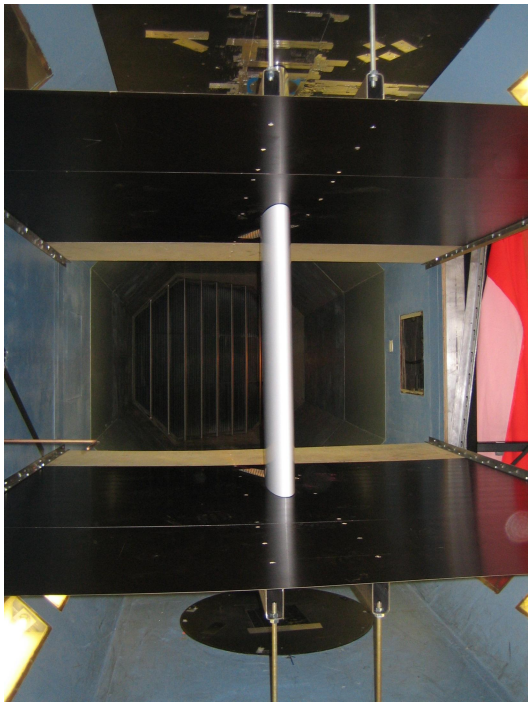

Fig. 4 Airfoil section in wind tunnel.

The wind tunnel tests were conducted mainly with two different wind speed by varying angle of attack. One test were done by varying wind speed between 30..55 m/s, the realized test program is shown in *Table 3*.

Table 3. Realised wind tunnel test program.

Test	Wind speed (m/s)	Angle of attack (º)	Control strategy	
			Temperature (ºC)	Strain (µstrain)
1	30	0, 2, 5	Off / 60	
2	44	0, 2, 4[a]	Off / 60	
3	44	2	55, 60, 65	
4	30 -55	0	60	
5	30	0		0 - 900

[a] Angle of attack should be limited because lift force exceeds the maximum force of weighting system

Effect of activation of SMA-wires on lift coefficient CL and lift to drag L/D force with different wind speeds and attack angles are shown in *Fig. 5*. Airfoil was heated by Joule heating gradually up to 60°C. It can be easily seen that activation of SMA wires causes a remarkable change in lift force with both wind speeds (30 m/s and 44 m/s) and with all angles of attacks. It can be noticed that the measured L/D is considerably lower than the theoretical L/D ratio of the profile, which is about 100. However, the difference is well explained by the factors of the test setup.

Some irreversible shape changes were detected during the first activation cycles. This is quite typical behaviour in SMA composites during the first's activation cycles. After some tens of cycles the behaviour of SMA composite is typically stabilized and this same behaviour is detected in wind tunnel tests.

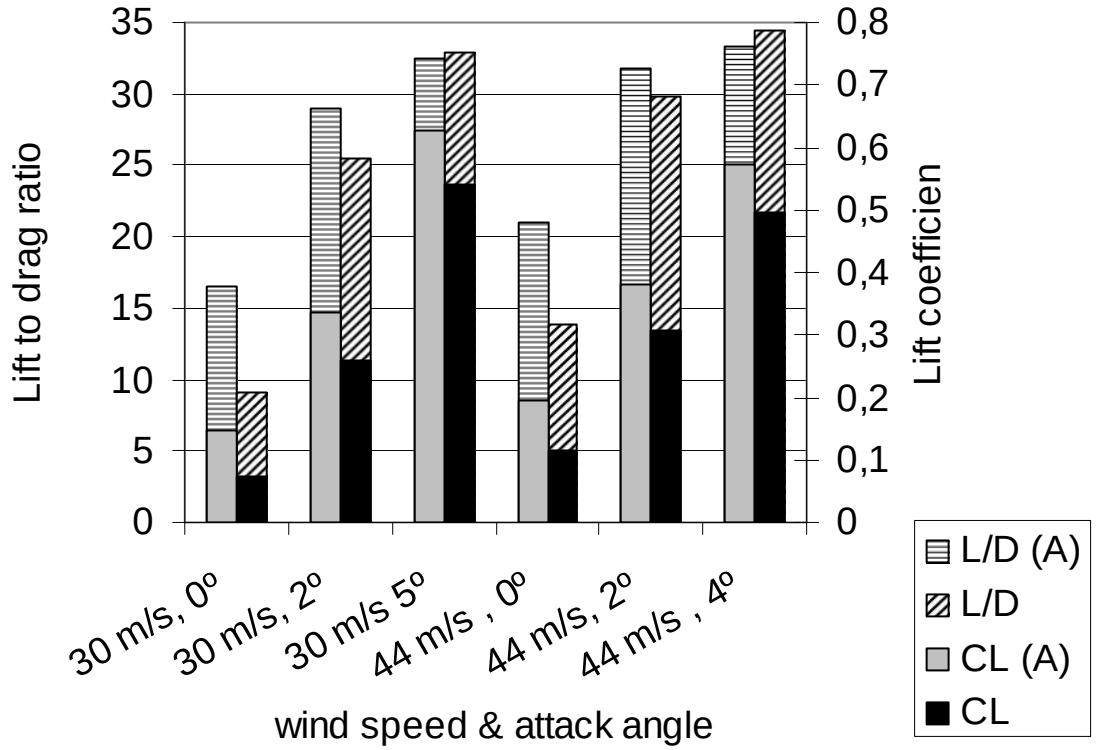

Fig. 5. Changes in lift force with different attack angles during the activation airfoil.

One of the most remarkable tasks in wind tunnel test was to establish the knowledge how the external load affects on achievable shape changes. In *Fig. 6* the differences in achieved strain levels and lift force between non-active and activated state with different wind speeds and attack angles are shown. Activation of the SMA wires creates almost equal increase of strain in lower skin (Strain 1) with all attack angles and both wind speeds. In upper skin (Strain 4) the increase of strain level is almost constant with attack angles 0º and 2º where increase of strain is a bit higher with higher wind speed of 44 m/s.

The most remarkable change in strain levels at upper skin happens with higher angle of attacks. In the case of wind speed of 30 m/s this change can be observed also in

lift force. Even though the strain level of upper skin increases with higher angles of attack, this change can't be seen in lower skin strain levels. One explanation of this behaviour could be that after certain strain level the mechanism of shape change is different.

This type of behaviour was observed in laboratory tests where after certain strain limit, the deformation of the upper skin starts to increase and deformation of the lower skin concentrates on to quite narrow area. It must be noted here that depending on the location of the strain gages, it is possible that this kind of deformation is not detected.

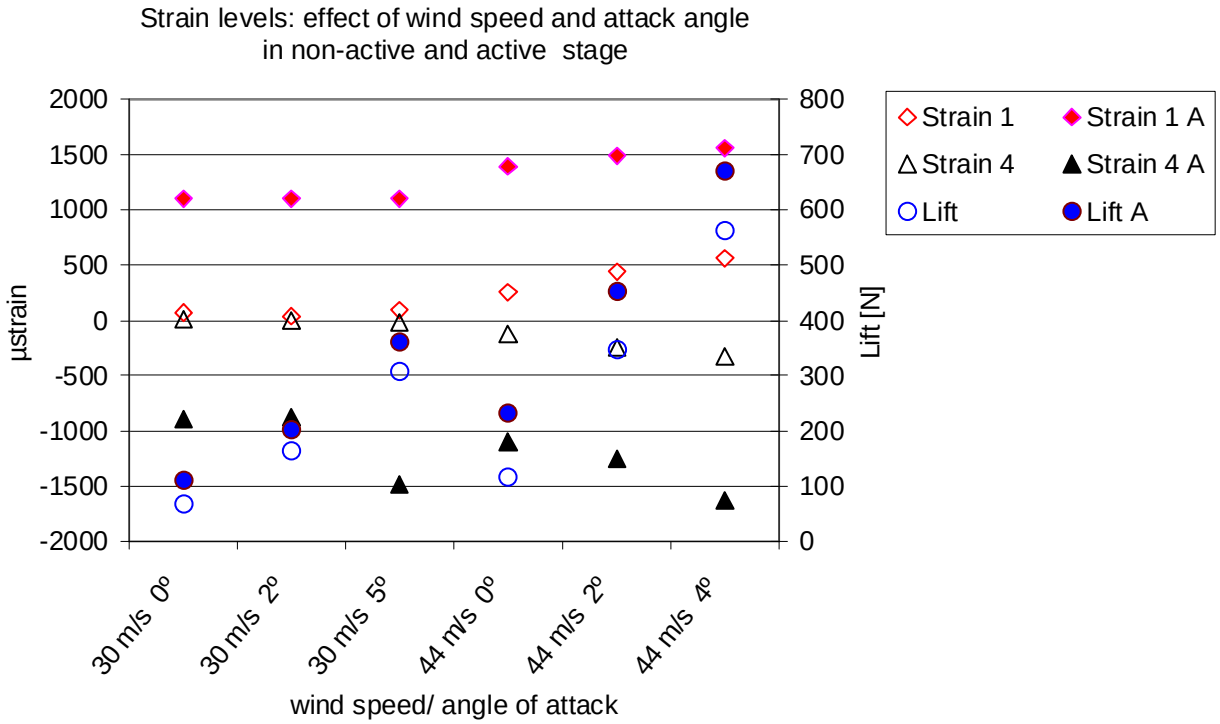

Fig. 6. Differences in strain and lift force levels between non-active and active state with different wind speeds and angles of attack.

In *Fig. 7* and *Fig. 8* the effect of activation temperature and wind speed on power consumption and achieved strain levels is studied. Increase of activation temperature from 55 ºC to 65 ºC has clear effect on lift force, which increases about 20 %. At the same time strain levels of the lower and upper skins are increasing about 10 % and 80 % respectively. The explanation of this non-uniform behaviour would be the same as in the case of higher angles of attack. The deformation mechanism changes in higher activation temperatures where the strain limit is also achieved.

The power consumption of this particular airfoil configuration at 55 ºC is approximately 2000 W and increases to 2500 W when the activation temperature is increased up to 65 ºC.

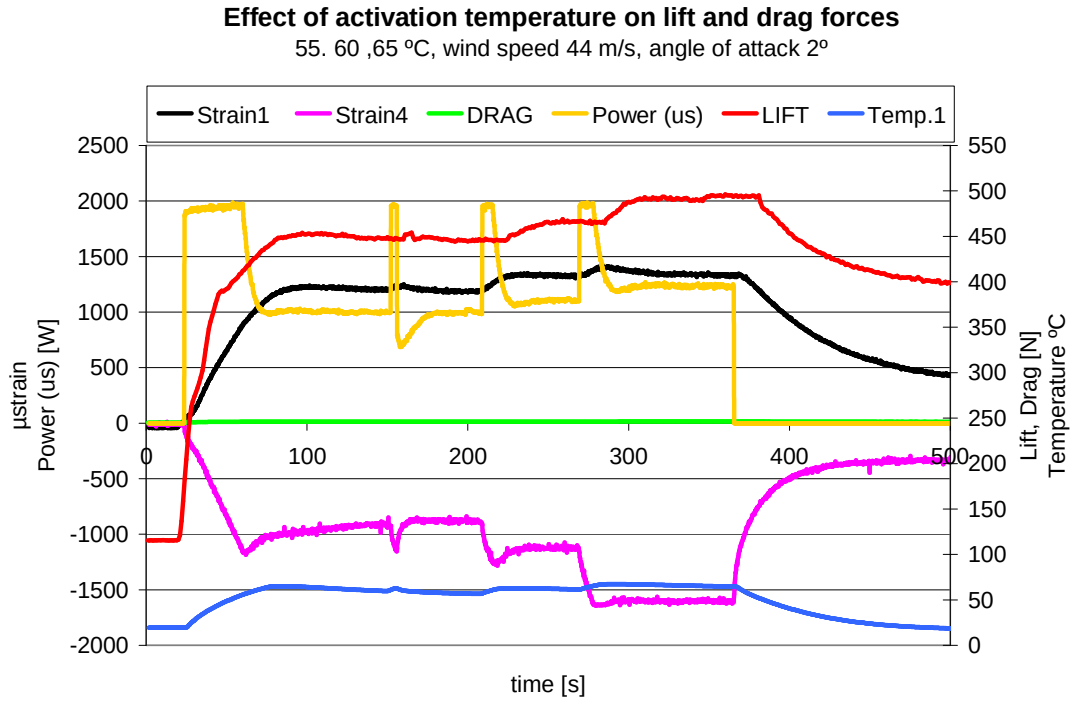

Fig. 7. Effect of activation temperature on achieved strain levels and power consumption.

The lift force, strain levels and power consumption increases gradually when the activation temperature is kept constant and wind speed is increased *Fig. 8*.

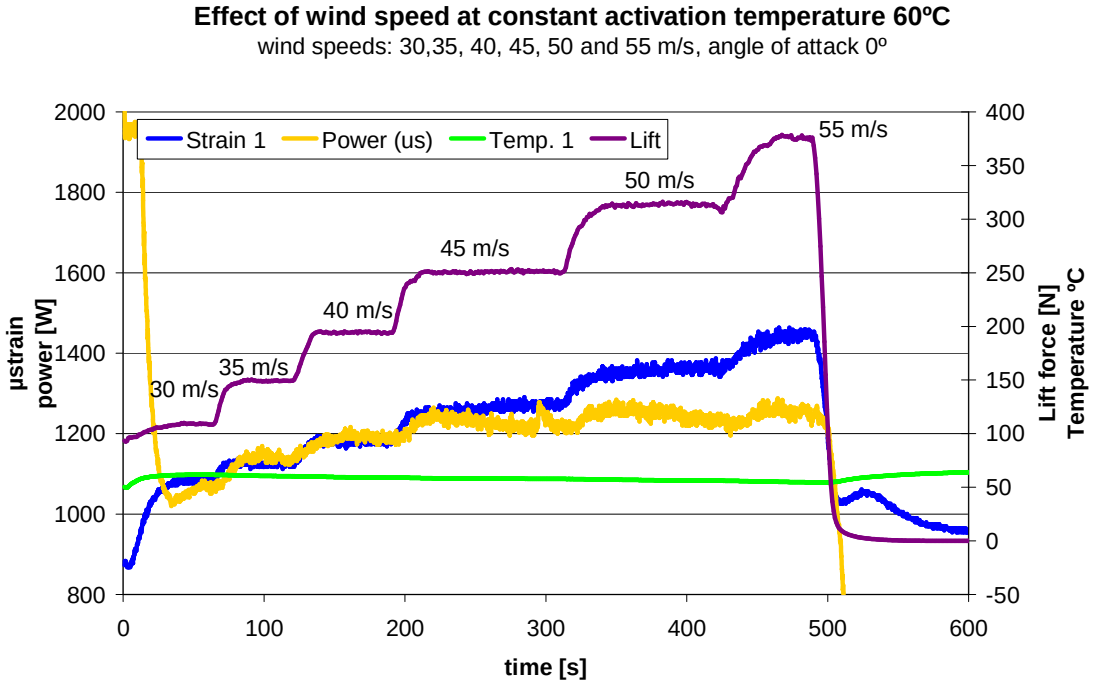

Fig. 8. The effect of wind speed on lift force and strain levels at constant activation temperature.

Controllability of the shape change was studied by varying target values of the strain levels by 300 µstrain steps. In *Fig. 9* it can be observed that strain levels of the skin laminates can be controlled quite accurately.

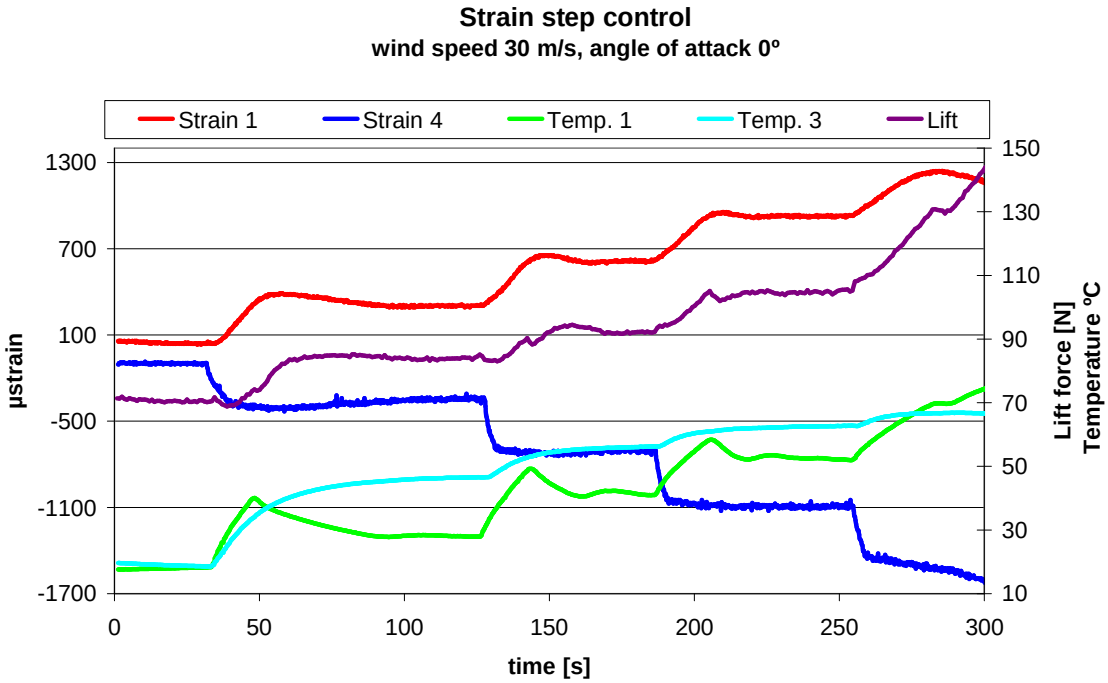

Fig. 9. Strain step controlled test where strain 1 was increased by 300 µstrain steps.

2.5 Conclusions

A novel type of adaptive wing profile was designed, manufactured and tested. Novel tools for designing and manufacturing of SMA actuated FRP composite structures were developed and demonstrated. The performance of the system was measured in laboratory conditions and also in wind tunnel. The developed control system works accurately for the shape control purpose of the airfoil in laboratory conditions. The changes in lift due airfoil activation were considerable. The changes in drag were not considerably large, therefore changes in the lift/drag ratio were favourable. The power consumption was not excessively high for wind turbine application. These results show the applicability of the system for wind turbine application in condition that the long term strength and durability of the system can be ensured. These issues will need further research and development.

The development of an adaptive structure is an iterative process that requires knowledge from many fields of engineering. An important part of the research work is the development of tools and manufacturing methods that can take the process closer to an industrial scale. Especially the modelling tools and the manufacturing processes need further development to make this kind of adaptive structures to be commercially accepted.

PART II: Adaptive modular blade based on R-phase transformation

3. R-phase transformation

One remedy to many of the problems encountered with embedded SMAs could be utilizing the R-phase transformation of NiTi. In the traditional NiTi materials there is an intermediate transformation from austenite to a rhombohedral phase and then another transformation to martensite. In traditional SMA designs the rhombohedral phase is ignored, because the deformation associated with this transformation is below 1.3 %. Inside composite laminates the strains this large cannot be applied without damaging the laminate. Therefore the R-phase transformation can be utilized.

The Clausius-Clapeyron constant determining the effect of stress on the phase transformation temperatures is much larger [17 MPa/K] for R-phase transformation than for martensitic transformation [5-6 MPa/K] and therefore the stress in the SMA wires does not shift the transformation temperatures as much as in martensitic transformation. The width of the phase transformation zone of R-phase transformation is also much smaller [2-10 K] than for the martensite transformation [25-30 K]. This means faster heating and cooling and smaller power consumption.

The R-phase wires with suitable R-phase transformation temperatures are produced from ordinary NiTi wires by a special heat treatment. The R-phase transformation has been studied much less than the martensite transformation and data regarding many engineering issues, for examples stability, is scarce. However it has been shown that regarding the conditions the functional fatigue behaviour of R-phase wires can be up to decades higher compared to conventional austenite martensite actuated wires. This will make utilization of R-phase transformation even more fascinating in adaptive composites.

4. Modelling

To achieve more optimal adaptive structure advanced modelling tools are developed and used in different levels of implementation. Heat transfer modelling was used to determine effect of placement of SMA wires inside composite on heating and cooling performance and further determining of maximum theoretical operating frequency. For the optimising of fibre layout and placement of SMA wire more accurate models describing actuator performance was developed.

4.1 Heat transfer modelling

The heat transfer analysis of the composite embedded SMA wire is applied to study the cooling time of the SMA wire heated composite windmill blade under surrounding laminar wind flow. The model is verified by time versus temperature wind tunnel measurement.

In this model the shape memory alloy wire is embedded at the depth of 0.3 mm from the laminar wind flow affected surface of the composite. Studies of cooling time ver-

sus the shape memory alloy wire embedding depth are carried out in the verification model. In this case the laminar flow speed is 30 m/s.

The model contains a total of two SMA wires, one full wire in the middle and the other is split lengthwise in two, one half in the right side and one in left. This configuration provides realistic temperature gradient during heat transfer.

The model is divided in three steps. In the first step the initial temperature is applied in the model. In the second step the SMA wire is heated according to the wind tunnel test results. Measured time versus temperature curve is applied in the model as a boundary condition for the middle one of the SMA wires.

In the third step heating is removed and the composite structure is cooled via convection at the composite surface. The cooling convection is governed by the laminar wind flow. For this there is added a film coefficient at the composite surface describing effect of the flow. The rest of the modelled surfaces are isolated.

The film coefficient is calculated by using following method. For these calculations three non unit parameters are determined which are Pradt, Reynolds and Nusselt number. Pradt number is

$$\mathrm{Pr} = \frac{c_p \mu}{k}. \tag{1}$$

In which c_p is fluid specific heat, μ is fluid viscosity and k is fluid conductivity. Reynolds number is

$$\mathrm{Re} = \frac{\rho u_\infty L}{\mu}. \tag{2}$$

In which ρ is fluid density, u_∞ is fluid free stream velocity and L is length of composite. Nusselt number is

$$\mathrm{Nu} = 0.664 \cdot \left(\mathrm{Pr}\right)^{\frac{1}{3}} \cdot \sqrt{\mathrm{Re}}. \tag{3}$$

The film coefficient is

$$h = \frac{k}{L}\mathrm{Nu}. \tag{4}$$

In this study four different fluid free stream velocities are added to the model. These velocities and corresponding Pradt, Reynolds and Nusselt numbers, as well as fluid viscosity and the length of plate are presented in the *Table 4*. Specific heat, density and conductivity for the composite, for the shape memory alloy wire and for the fluid are presented in the *Table 4* and *Table 5*.

Table 4. The laminar fluid flow parameters

		Unit		Unit		Unit		
Length of plate	0.087	m	15	mm				
Fluid viscosity	0.000017	kg/m*s	0.017	cP	0.00017	P		
Fluid density	1.29	kg/m^3						
Fluid specific heat	1.007	kJ/kg*K						
Fluid conductivity	0.02569	W/m*K						
Pradt number	0.666368							
Reynolds number upper limit for laminar flow	300000							
Fluid free-stream velocity	5	m/s	20	m/s	30	m/s	45	m/s
Reynolds number	33008.82		132035.3		198052.9		297079.4	
Reynolds number validity	ok		ok		ok		ok	
Nusselt number	105.371		210.742		258.1052		316.1131	
Heat transfer coefficient	31.11473	W/m^2*K	62.22946	W/m^2*K	76.21521	W/m^2*K	93.34419	W/m^2*K

Table 5. Parameters for the composite structure and the shape memory alloy wire

Shape memory alloy specific heat	837.36	J/(kg*K)
Shape memory alloy conductivity martensite	18	W/(m*K)
Shape memory alloy conductivity austenite	8.6	W/(m*K)
Shape memory alloy density	6450	kg/m^3
Composite specific heat	1100	J/(kg*K)
Composite conductivity	1	W/(m*K)
Composite density	1400	kg/m^3

In the *Fig. 10* and *Fig. 11* temperature gradients are shown at the different stages of the analysis. In these results fluid flow velocity is 30 m/s and the shape memory alloy wire is embedded at 0.3 mm depth from the surface. Comparison between the shape memory alloy wire composite verification model and wind tunnel measurement is presented in the *Fig. 12*. In the verification model heat flux is calculated. Time versus temperature behaviour is shown in the *Fig. 13*

The effects of cooling time at different fluid flow velocities are shown in *Fig. 14*. The element mesh is unchanged in verification and rapid heating models but the film coefficient is changed at the surface of the SMA wire composite model according to *Table 4*, except rapid heating model in which 5 m/s and 45 m/s fluid flow velocities are studied.

In the figures the temperature response is taken from the same node of the SMA wire. This qualifies heat flux in the composite. The study of cooling time versus different embedding depths of the shape memory alloy wire causes geometry changes in the verification model. For this reason element mesh is changed and in the *Fig. 16*, the

temperature response is taken from SMA wire, however the location of the nodes are slightly different between each embedding depth.

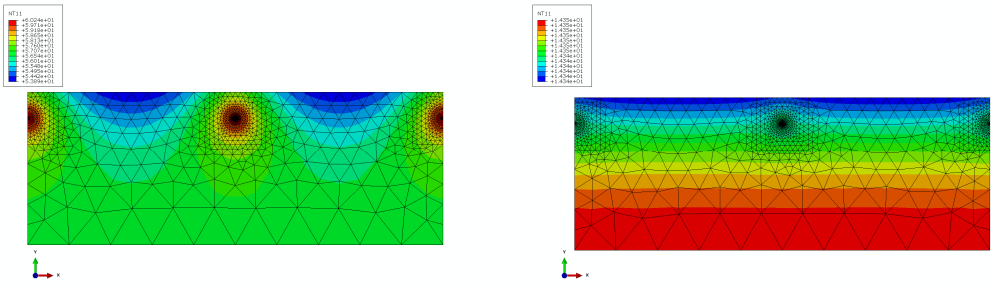

Fig. 10 Verification model temperature gradients after heating and after cooling.

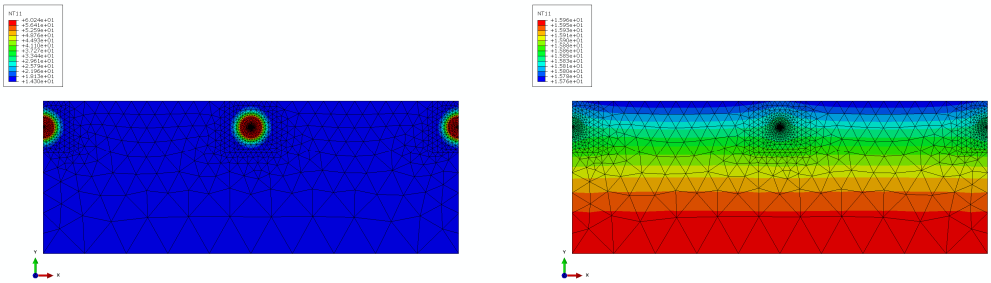

Fig. 11 Rapid heating model temperature gradients after heating and after cooling in the rapid heating model

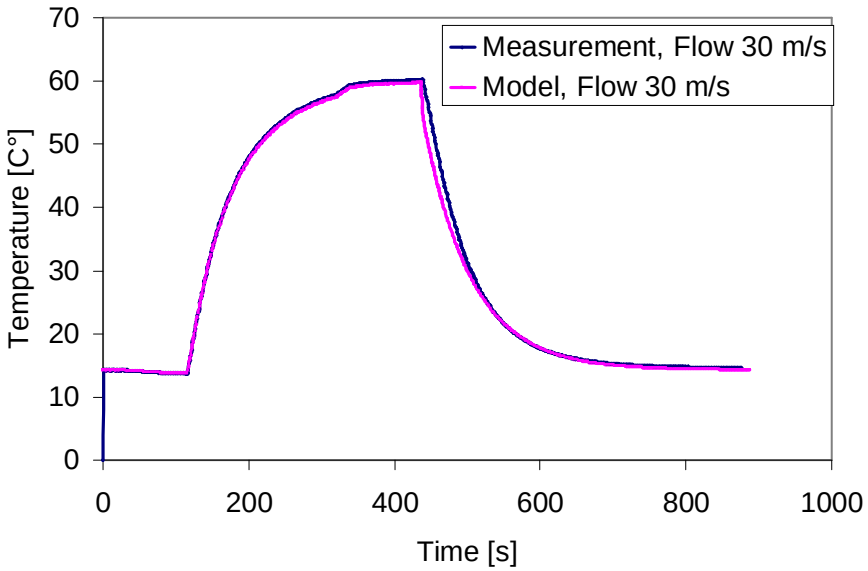

Fig. 12. SMA composite model versus wind tunnel measurement

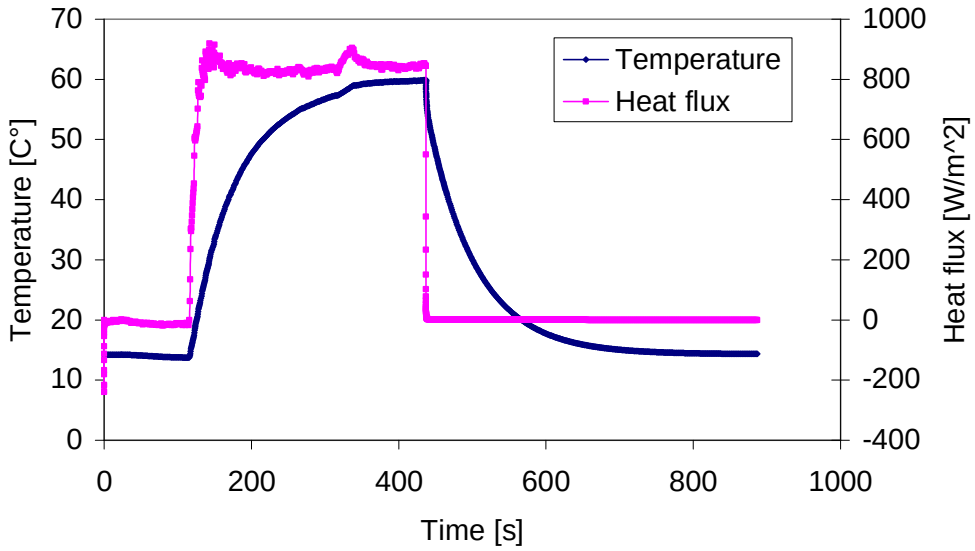

Fig. 13 Behaviour of temperature and heat flux during 30 m/s laminar wind flow

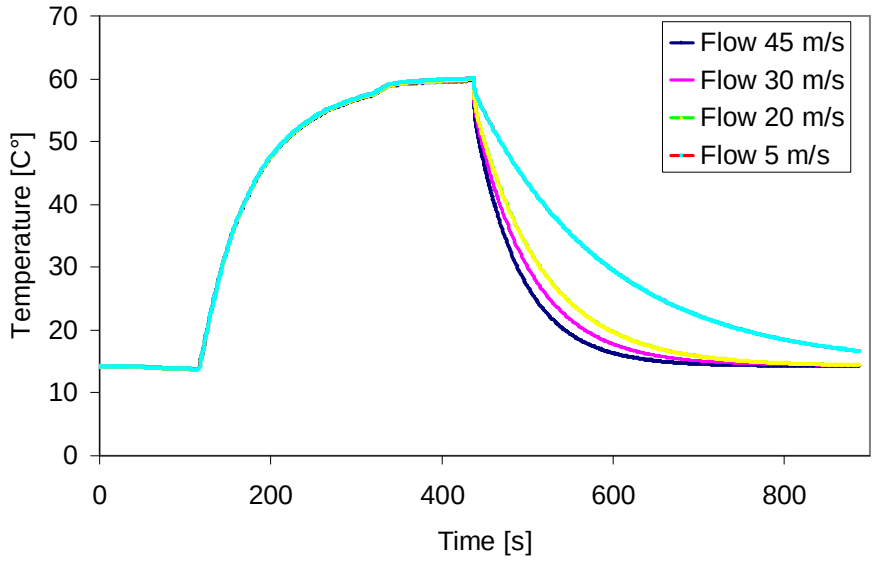

Fig. 14. The temperature curves with respect of fluid flow velocities

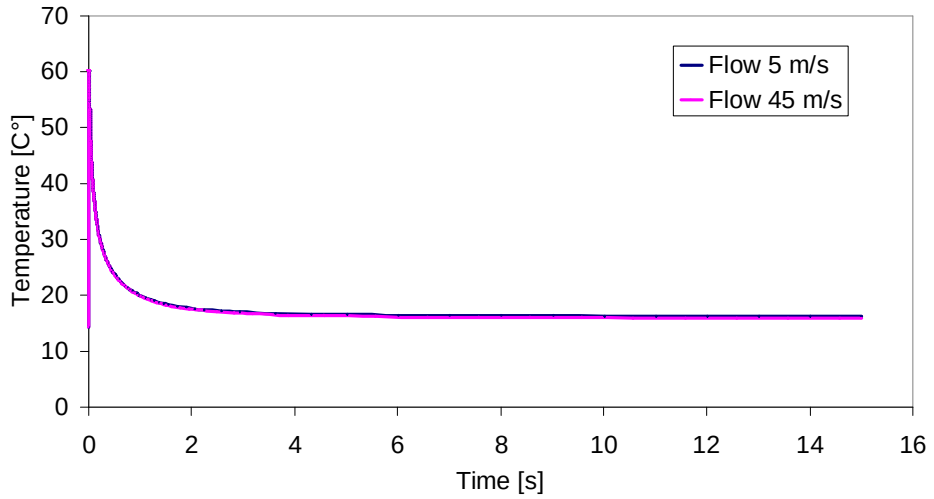

Fig. 15. The temperature curves in the rapid heating model

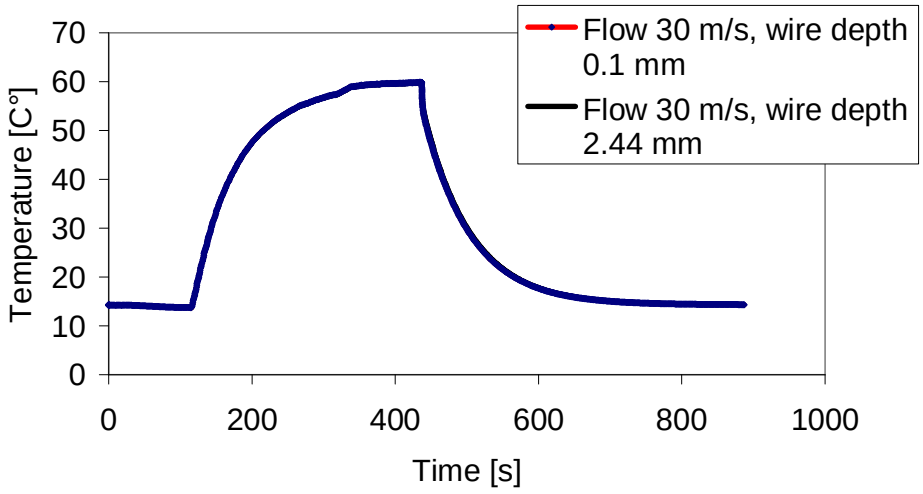

Fig. 16. The cooling time versus embedded depth of the shape memory alloy wires. Cooling of the wire is independent of embedded depth and the curves are identical.

4.2 Conclusion

The shape memory alloy wire composite model is corresponding well with time versus temperature measurements in wind tunnel. At the beginning of the cooling step the time versus temperature curve is steeper than measured, however the latter time versus temperature curve given by the SMA wire composite verification model coincides well with measurement. According the *Fig. 14* the different fluid flow velocities have a recognizable effect in the cooling time.

The rapid heating model cools down to 15 C° in a few seconds. However the cooling time to reach equilibrium with ambient temperature is longer than shown in *Fig. 15*. According the results of the rapid heating model fluid flow, the velocities do not affect significantly in the cooling time. In this light, the major portion of the released energy by heated shape memory alloy wire is consumed to increase composite temperature by a few degrees.

4.3 Modelling of NiTi SMA wire actuators

Sophisticated modelling tools were developed For the more appropriate material model for describing SMA wire behaviour in actuator use. The program iRLOOP developed by IT ASCR has the following main features for simulation of shape memory material response to uniaxial mechanical and thermal loading:

- The transformation kinetics is not simulated but obtained directly from experimental datasets.
- An adaptation of a Duhem-Madelung model is used to simulate the SMA responses in partial internal cycles.
- Non-hysteretic transformation behaviour of austenite and martensite phases is introduced, which enables to fit the internal loops in thermal cycles and actuator cycles reliably.
- The model captures SMA responses due to deformation processes in martensite state (reorientation, detwinning etc) by introducing new approach, which avoids use of the problematic concept of thermal and stress induced martensites commonly utilized in the literature.

In order to fit the model to particular material behaviour (*behavior of NiTi wires is varying dramatically with respect to the wire chemical composition and heat treatment*), a new program – iRLOOP fit – was created. By changing of 21 internal parameters: 5 material parameters (2 elastic moduli, maximum transformation strain in tension and in compression, critical slope) and 16 parameters for definition of transformation and reorientation kinetics, we are able to capture with good quantitative agreement both superelastic and memory behaviour of NiTi wire.

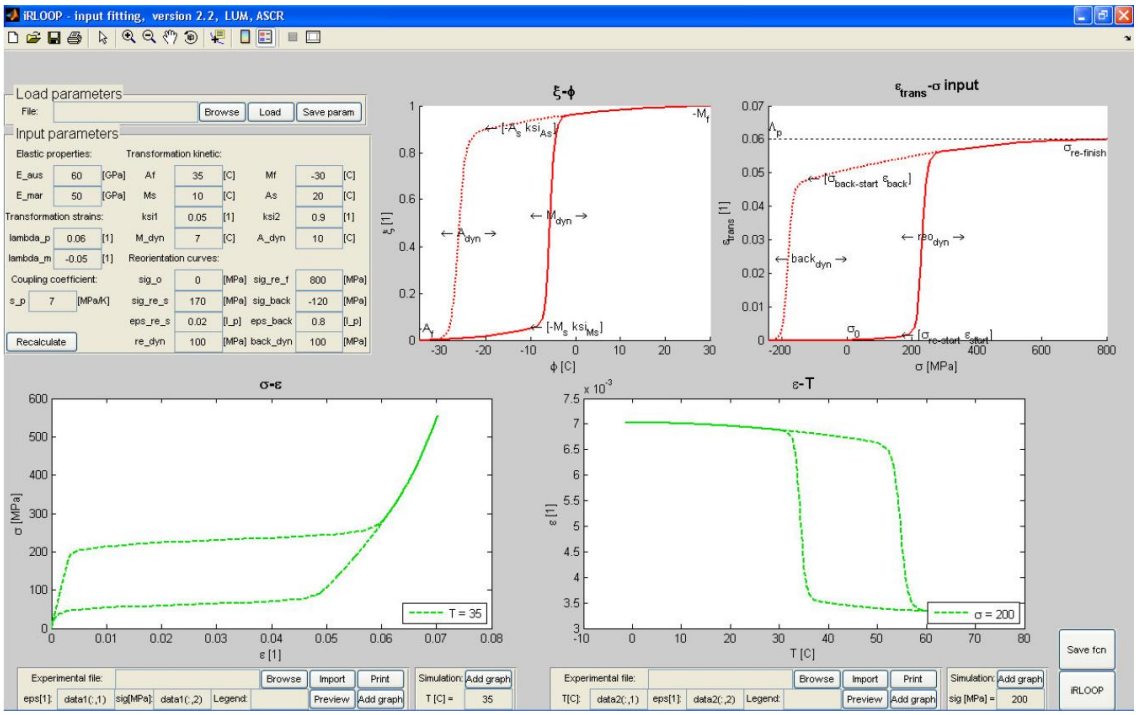

Fig. 17. *Graphic window of iRLOOP-fit program.*

Using this new fitting tool, we achieved a very accurate simulation of NiTi actuator cycles Fig. 18, which is crucial for design of active composites with embedded NiTi wires.

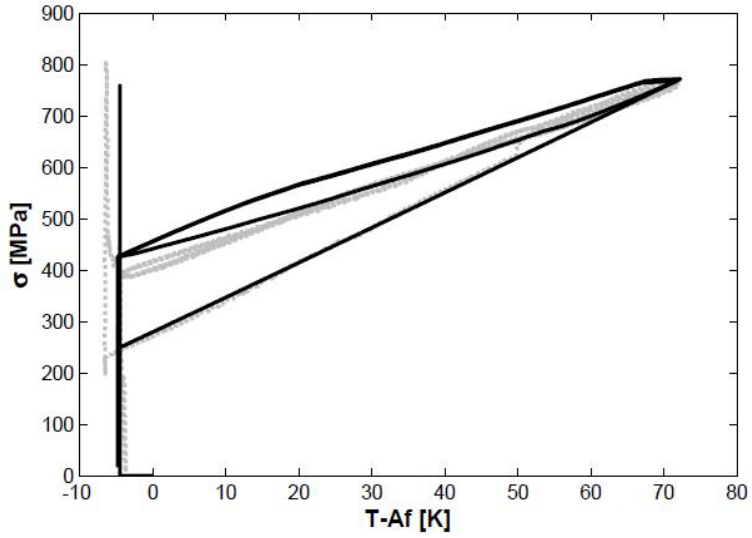

Fig. 18. *Recovery stress test (actuator mode). Experiment is marked by dashed lines, simulation by full lines.*

In order to simulate comprehensive structures, the proposed model was implemented to Abaqus as a User programmed material model, Umat, written in Fortran. Currently a simplified Jacobian is used. Laminate structures are usually modelled using the **shell section, composite* option in Abaqus. The **rebar layer* option, originally created for modelling steel reinforcement in concrete structures, was used for integrating the 1D SMA material model into 3D composite shell models. The numerical implementation and modelling of laminate structures was performed in collaboration with VTT and ASCR.

4.4 Modelling of a R-phase actuated trailing edge

The behaviour of the R-phase memory shape alloy wire is modelled by using a negative thermal expansion coefficient due to lack of a sufficient r-phase memory shape alloy wire material model. The negative thermal expansion coefficient includes a real thermal expansion of heating but also phenomena related with the behaviour of the R-phase memory shape alloy wire. The later one could be studied with a model which simulates the results of a memory shape alloy wire thermal treatment experiment. In this model and experiment one end of the memory shape alloy wire is fixed and the other is attached to a spring. A single quadratic truss element is applied in an analysis. A predefined temperature 20 °C is set for the element before the analysis and a thermal load increases from 20 °C to 60 °C in the element during the analysis.

In this model two different parameters could be modified. The first one is the negative thermal expansion coefficient and the second one is the spring stiffness. These parameters are defined to provide 400 MPa stress and 0.6 % strain in the memory

shape alloy wire. The defined negative thermal coefficient is used in a wing deformation analysis.

Table 6. The parameters of the memory shape alloy wire analysis

Temperature variation	20-60	°C
Stress after thermal treatment	400	[MPa]
Strain aster thermal treatment	0.6	%
Young's modulus	30	[GPa]
Poisson ration	0.3	
Equivalent spring stiffness	130000	[N/m]
Equivalent negative thermal expansion coefficient	-0.0005	

The geometry of the wing model is equivalent with NACA 63-215 airfoil. The model consist three different parts which are the support foam, the adhesive bonded wing tip and the composite structure. These different parts are represented in the *Fig. 19*.

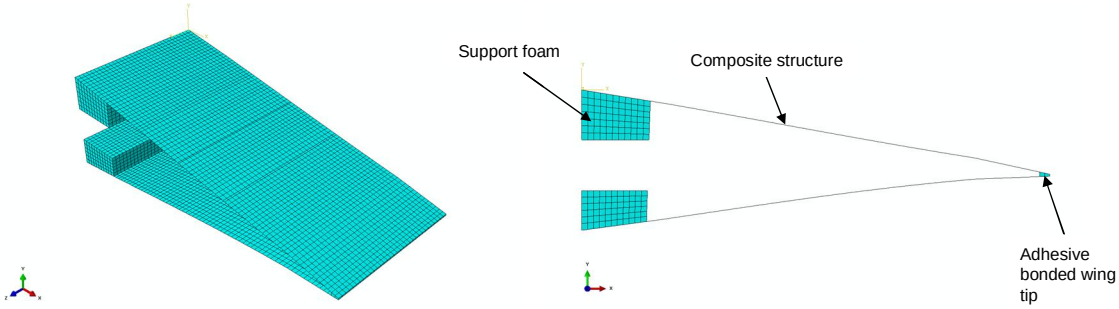

Fig. 19. The analyzed wing model

The composite structure of the wing is compounded of the glass fibre, the UD glass fibre, and the Kevlar-45 woven mat ply layers. The R-phase memory shape alloy wires are modeled as a rebar layer. In the *Fig. 20* is represented a schematic picture of the composite structure and the r-phase memory shape alloy wires. The orientation of the glass fibres and Kevlar-45 woven mat are ± 45° and UD glass fibres are orientated respect to a length direction of the wing. The orientations of different layers are represented in the *Fig. 21*. The spacing of the R-phase memory shape alloy wires is 0.004 mm and the wires are orientated 90° respect to the length of the wing. The thickness of the composite structure varies according Fig. 20 and the thickness values are represented in the Table 7.

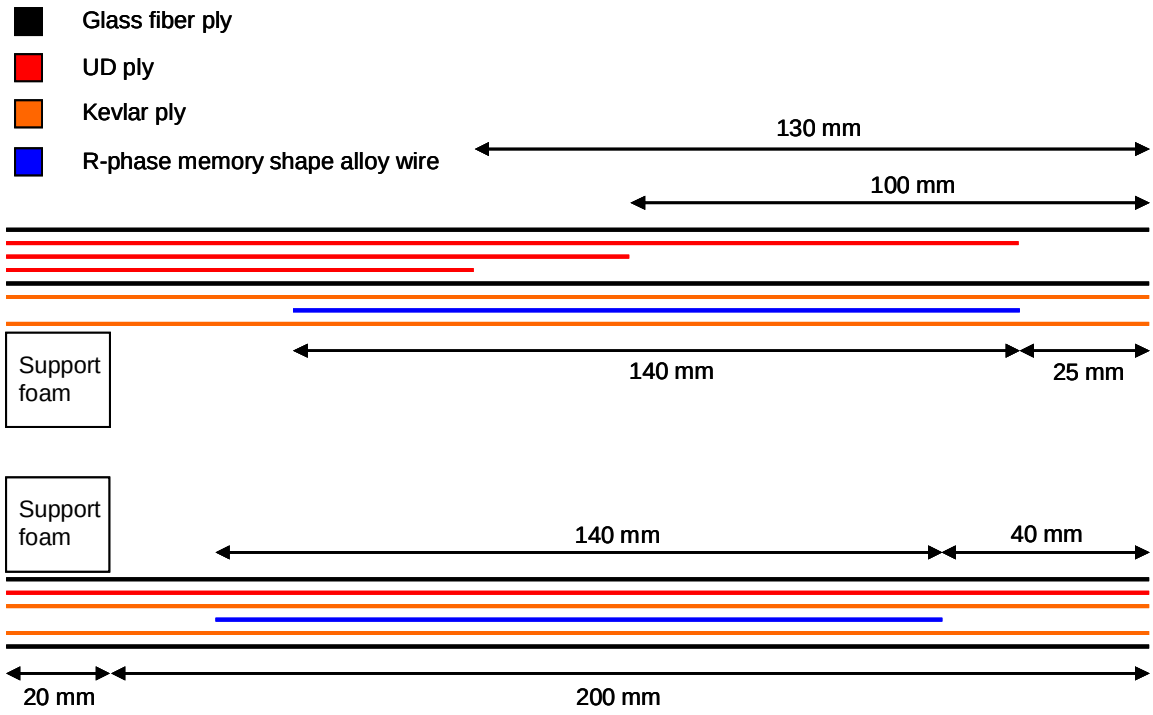

Fig. 20. A schematic picture of the composite ply layers

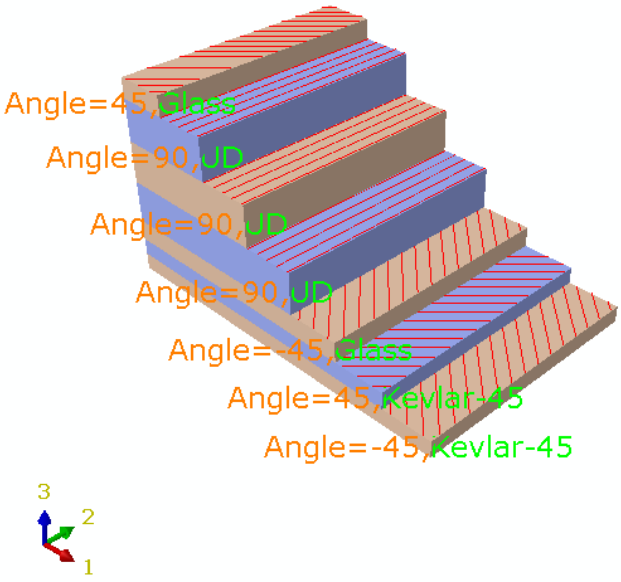

Fig. 21. The ply stack plot

Table 7. Ply thickness values and rebar locations

Upper surface of the wing Thinnest ply stack	Number of the plies	Thickness	Unit
Kevlar-45 woven mat	2	0.00046	[m]
Glass fibre	2	0.00056	[m]
Total thickness		0.00102	[m]

Thin ply stack	Number of the plies	Thickness	Unit
Kevlar-45 woven mat	2	0.00046	[m]
Glass fibre	2	0.00056	[m]
UD glass fibre	1	0.00058	[m]
Total thickness		0.0016	[m]
Middle plane		0.0008	[m]
Rebar distance from middle plane		0.0007	[m]

Medium ply stack	Number of the plies	Thickness	Unit
Kevlar-45 woven mat	2	0.00046	[m]
Glass fibre	2	0.00056	[m]
UD glass fibre	2	0.00116	[m]
Total thickness		0.00218	[m]
Middle plane		0.00109	[m]
Rebar distance from middle plane		0.00099	[m]

Thick ply stack	Number of the plies	Thickness	Unit
Kevlar-45 woven mat	2	0.00046	[m]
Glass fibre	2	0.00056	[m]
UD glass fibre	3	0.00174	[m]
Total thickness		0.00276	[m]
Middle plane		0.00138	[m]
Rebar distance from middle plane		0.00128	[m]

Lower surface of the wing	Number of the plies	Thickness	Unit
Kevlar-45 woven mat	2	0.00046	[m]
Glass fibre	2	0.00056	[m]
UD glass fibre	1	0.00058	[m]
Total thickness		0.0016	[m]
Middle plane		0.0008	[m]
Rebar distance from middle plane		0.0007	[m]

The support foam and the adhesive bonded wing tip are modeled by using an isotropic elastic material model and a quadratic 3D element. However in the composite structure an elastic lamina material model with engineering constants and a shell ele-

ment is applied. The material parameters of the models are shown in the *Table 8* and *Table 9*. As mentioned earlier predefined temperature is 20 °C and the thermal load increases from 20 °C to 60 °C during the analysis. Results of this analysis are represented in the *Fig. 22* and *Fig. 23*.

Table 8 Young's modulus and Poisson's ratio of the support foam and the adhesive

	E	Unit	v
Foam	0.2	[GPa]	0.2
Adhesive	1	[GPa]	0.43

Table 9 Young's modulus, Poisson's ratio and shear modulus of the composite structure

	E_1	Unit	E_2	Unit	v_{12}	Unit	G_{12}	Unit	G_{13}	Unit	G_{23}	Unit
Kevlar-45 woven mat	22	[GPa]	22	[GPa]	0.06	-	1.4	[GPa]	1.4	[GPa]	1.4	[GPa]
Glass fibre	20.5	[GPa]	20.5	[GPa]	0.11	-	4	[GPa]	4	[GPa]	4	[GPa]
UD glass fibre	32	[GPa]	9	[GPa]	0.26	-	4	[GPa]	4	[GPa]	4	[GPa]

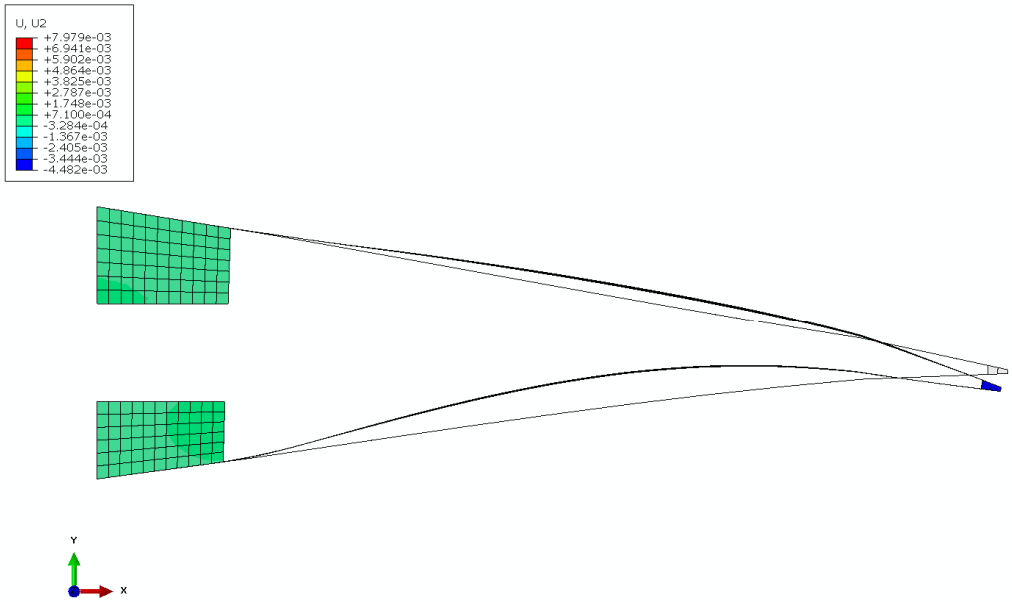

Fig. 22. The deformed wing and the non deformed wing

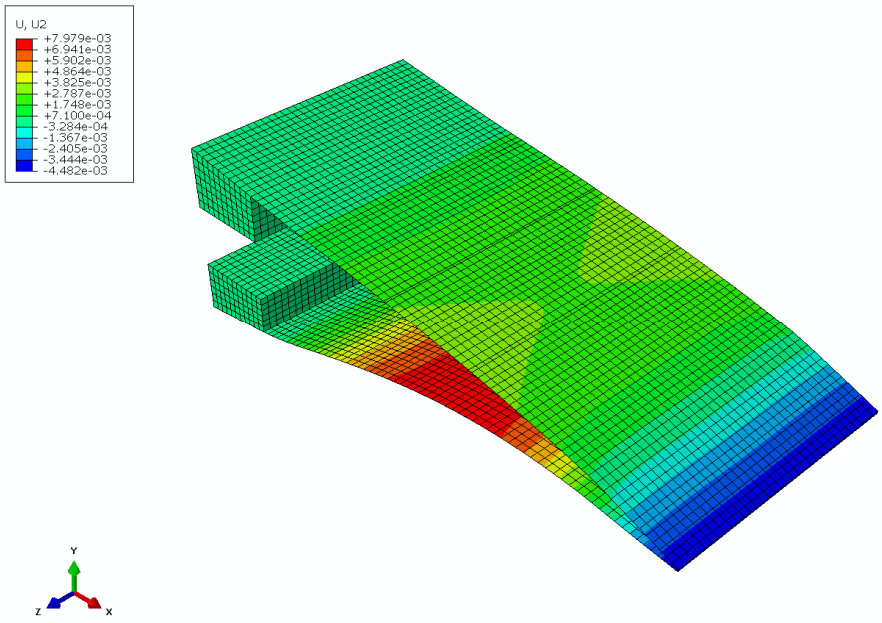

Fig. 23 The deformed wing

5. Pressure sensors for detection disturbance in airflow

In order to react to changes in operating environment, suitable sensors are needed to give feedback to control system of adaptive parts. The goal was to find out would it be possible to detect improper air flow on surface of the wind turbine blade by sound pressure sensors attached to the surface of the blade. A wind turbine blade profile sample was instrumented with custom made EMFi-microphone (Electro Mechanical Film) strip which contained five independent microphones. EMFi-microphone is dynamic sensor where changes in pressure can be detected. Total pressure level cannot be determined without extra devices. Amplifiers for EMFi-microphones were made at VTT.

To avoid too complex measurement system, the EMFi-microphones were not assembled to an adaptive modular airfoil. Measurements were carried out at VTT in small icing wind tunnel. Two parameters were varied in the wind tunnel tests, velocity of air flow, three constant velocities 10, 20 and 30 m/s (i.e. 36, 72, and 108 km/h, respectively), and blade angle in steps from -20° to + 20°.

5.1 Test setup and measurements

Blade profile was installed into wind tunnel, side view and measurement points are shown in *Fig. 24*. The angle of attack has changed manually by turning a bar attached to blade.

Five thin wires were attached on the surface of the plate, fixed at one end (see *Fig. 24*). These wires will show the air flow turbulence. Blade was video recorded during the measurements in the wind tunnel.

The air flow speed was set to constant value and blade angle was varied from chosen extreme to other chosen extreme. Each angle setting was kept for approximately two minutes. All signals was recorded simultaneously and continuously all the time when the blade angle was varied according the steps given in *Table 10*. This gives the effect of blade angle at given air flow speed in one measurement record. The start and end time of each angle setting was noted as seconds from start of the measurement.

Table 10. Measurements at 10 m/s

Date	23.7.2010	
Temperature	22,70	°C
Relative hum.	39,00	%
Flow velocity	10	m/s
Data stored to TestLab run:		
Run_1_10_m_s		

Wing angle	Measurement time	
°	start s	end s
-20	0	145
-15	145	270
-10	270	360
-5	360	480
0	480	600
2	600	720
4	720	840
6	840	960
8	960	1080
10	1080	1200
11	1200	1320
12	1320	1440
13	1440	1560
14	1560	1680
15	1680	1800
20	1800	1920

Colour map describes signal amplitudes at 10 m/s wind speed with different frequencies. Angles of attack are shown in *Fig. 24*. As expected signal levels are increasing with angle of attack when level of turbulent flow increases.

It can be seen that air flow changes turbulent when angle of attack 10° is achieved, low frequency signals are increased in all microphones. Signals are gradually increasing when angle of attack is changed with one degree steps. When angle of attack is increased from 15° to 20° strong turbulence can be detected at the whole frequency band at microphone 5. In other microphones the change is also easily seen but the strongest signals can be detected at lower frequencies.

Measurement principle was detected to very potential for measuring air flow fluctuations directly on airfoil surface.

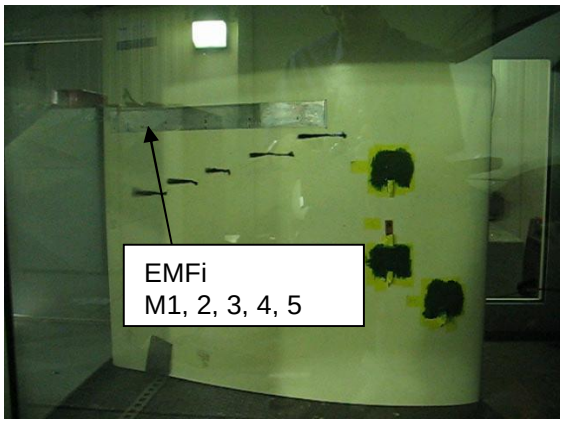

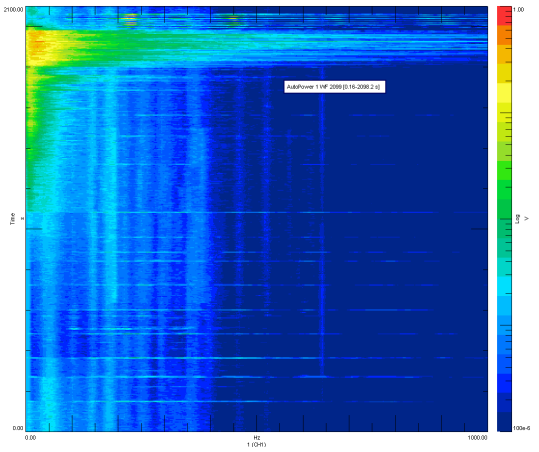

M1

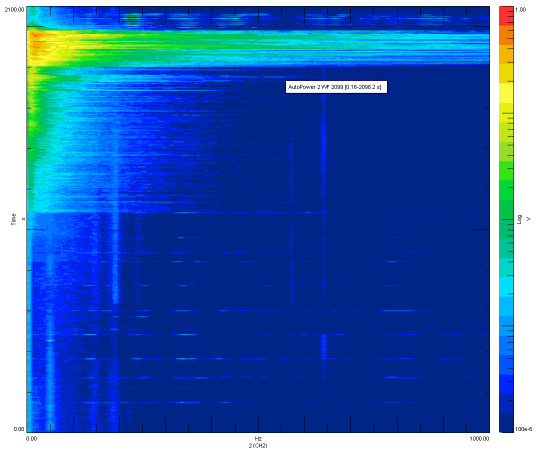

M2

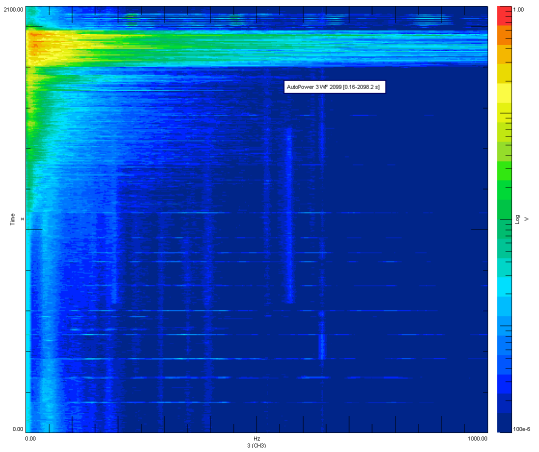

M3

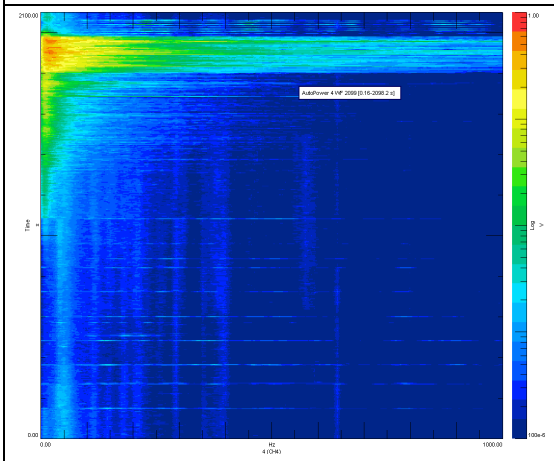

M4

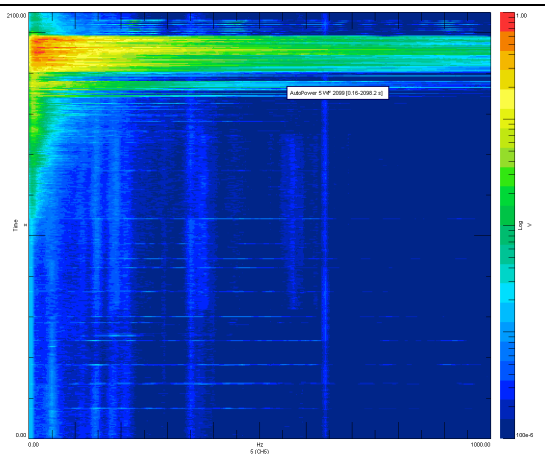

M5

Fig. 24. Test setup and Colormasp of EMFi-microphones 1-5 signal from 10m/s measurement. X-axis frequency 0 – 1000 Hz, Y-axis measurement time (blade angle increases with time). Colors indicate signal amplitude.

6. Designing and manufacturing of modular structure

When the complexity of structures is increasing, so does the demand for easy and cost efficient maintenance. Utilization of adaptive systems in wind turbine blades requires robustness for the systems, especially reliability and safe behaviour in possible malfunction situations. Because the life cycle of wind turbine blades is rather long, it is essentially important to design the new systems to be easily replaceable.

From these points of view, the development for a modular design for an adaptive trailing edge was launched. The principal idea was to realize plug-and-play type of adaptive modular part where all the sensors, actuators and other sensitive components are installed. In this way the required adaptive functionality could be realized along with an easily replaceable part, and possible malfunctions would not be so critical for the operation. The principle of modular trailing edge is shown in *Fig. 25* and the first small scale prototype is shown in *Fig. 26*.

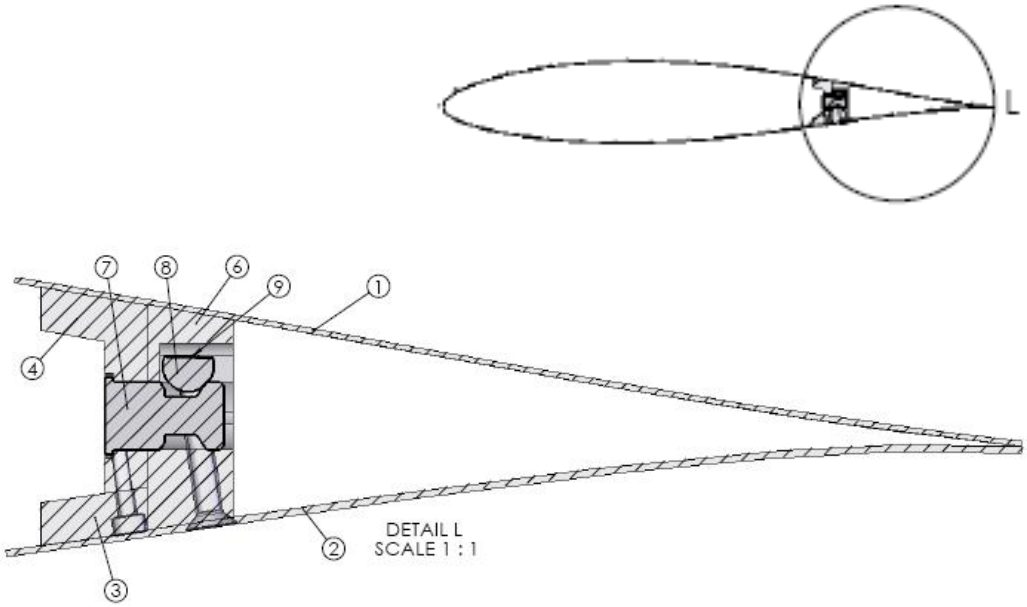

Fig. 25. Principle of a modular plug-and-play type trailing edge

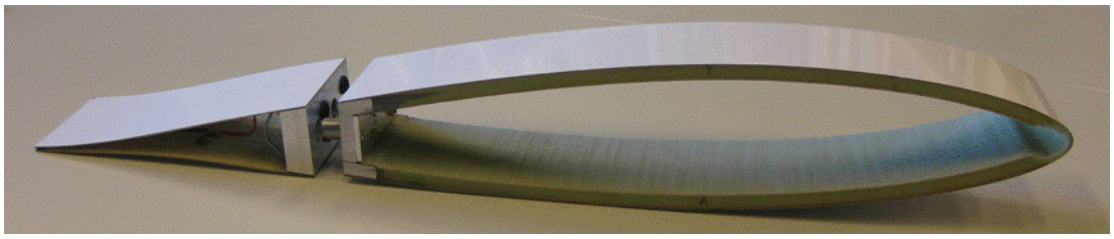

Fig. 26. The first prototype of a modular trailing edge.

7. R-phase actuated adaptive composites

7.1 Manufacturing R-phase composites

The development of the active WT blade airfoil using SMA-FRP composites was continued by utilizing R-phase wires. R-phase transformation has significantly smaller hysteresis and it exhibits superior resistance against functional fatigue compared to conventional SMA's based on martensite-austenite transformation.

Special manufacturing route is needed to realize R-phase actuation in composites. In manufacturing process, the pre-strain of wire should be below 1%. If this strain level is exceeded, the phase transformation is changing to traditional austenite martensite transformation.

In *Fig. 27* the behavior of R-phase wire in tensile test is presented; a) at room temperature where detwinnig of R-phase (inside red box) and martensite can be observed and b) at temperature higher than Md temperature where mechanical twinning of austenite is restricted.

a)

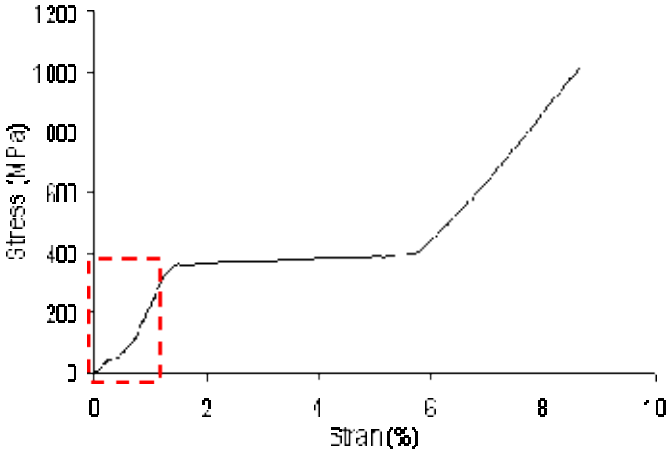

b)

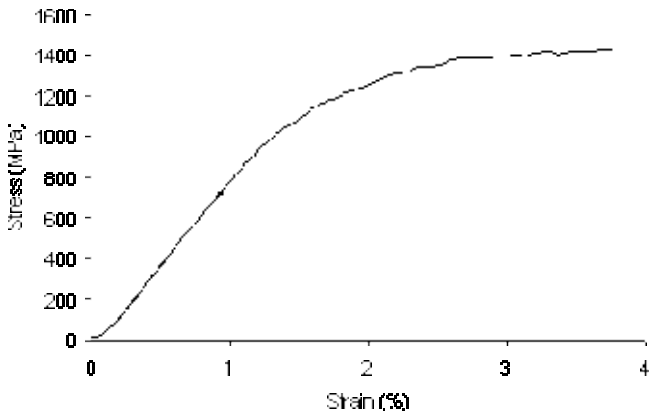

Fig. 27. Behaviour of R-phase wire under tension a) at room temperature b) after Md temperature. Area inside red box is showing R-phase orientation.

In practice, the pre-strain of the wire should be kept inside of the red box for realization of proper R-phase transformation. The manufacturing route was designed so that wires were heated up to 150°C (which is higher than MD) and after that loaded with 400 MPa stress, leading to approximately 0.7% of strain for wires. The wire setup was then embedded between aramide fabrics with heat curable epoxy and cured by hot pressing. When the laminate is cooling down, the stresses in R-phase wires are relaxed and only small portion of elastic stress remains. The special manufacturing jig is designed where each pair of wires is pre-strained by individual springs *Fig. 28* .

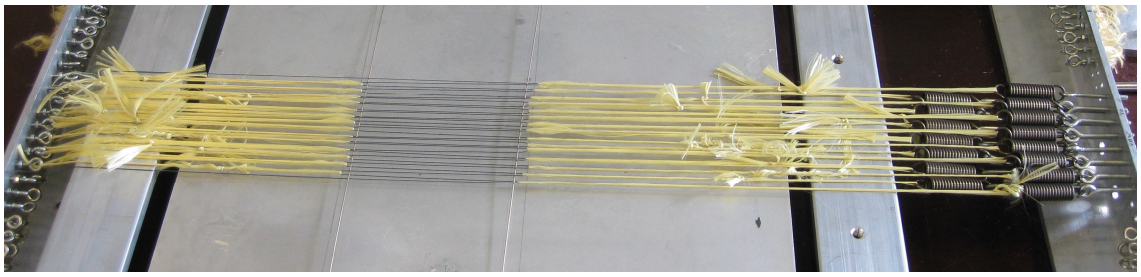

Fig. 28. Spring loaded manufacturing jig for R-phase composite production.

The behaviour of R-phase actuated modular trailing edge was studied as a function of temperature. Preliminary measurements concerning the actuation frequency were also conducted. The results of the tests are shown in *Fig. 29*.

According to these tests, R-phase transformation can induce the same size deflection to trailing edge as detected earlier in the case of conventional SMA's. The hysteresis of trailing edge is about 30 °C which is almost 20 °C smaller than detected earlier. Response of trailing edge against short electrical heating pulse is relatively fast. Approximately 1 s cycle time was achieved, but one should notice that because of heating of the matrix, some amount of deflection is remaining after each activation cycle until the whole structure is eventually fully heated up above R-phase activation temperature.

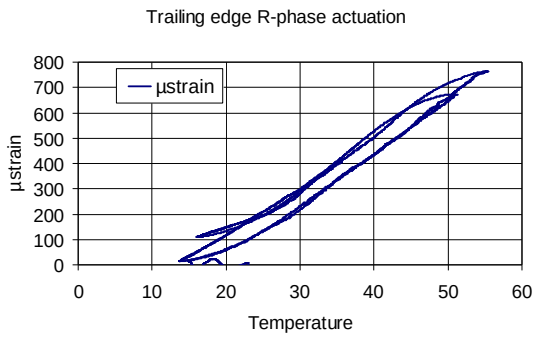

a)

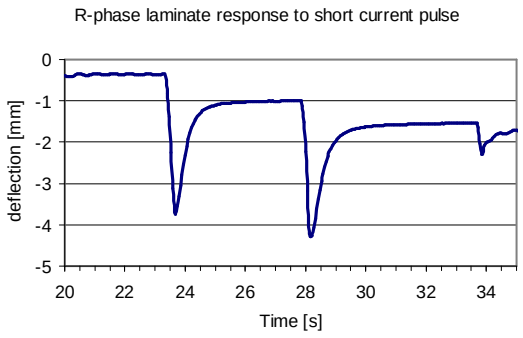

b)

Fig. 29. Response of R-phase actuated trailing edge as function of a) temperature and b) heating pulse.

7.2 Manufacturing of prototype for wind tunnel measurement

For the wind tunnel measurement, a modular prototype with 700 mm span length and 700 mm chord was manufactured. Leading edge part is consisting of sandwich structure having 10 mm Airex core and 1.2 mm thick glass fibre skin laminates. The connection part for trailing edge was machined from aluminium because of easy machining. In real application also the connection part can be manufacture from fibre reinforced composite. Joint interface is installed with the needed mechanical and electrical connectors for powering of actuators and collection of sensor signals.

The trailing edge part was manufactured based on modelling results represented in chapter 4.4, layout of adaptive laminate structures is presented in *Fig. 20* and *Fig. 21*. The manufacturing route of trailing edge was similar to the airfoil based on conventional SMA composite. In the first step the adaptive laminates were manufactured as described in previous chapter. After curing of adaptive laminates, extra ply layers were laminated to adaptive laminates. Adaptive skin laminates were bonded to female connection part after the strain gages and temperature sensors were assembled.

One thermocouple was bonded on both upper and lover skin laminates in the middle of SMA wire region. Strain gages were assembled on active area (3 strain gages for lower skin laminate and 2 for upper skin). In *Fig. 30* a modular prototype ready for preliminary testing is presented. Connectors for actuator powering and sensors can be seen in both ends of the joint interface.

Fig. 30. Adaptive modular airfoil prototype based on R-phase actuated SMA composites

8. Testing

Testing of the prototype was made in two steps. First part of testing was conducted in laboratory to evaluate functionality of prototype without airflow. Second part of the test was done in VTT icing wind tunnel to evaluate how adaptive airfoil works under different airflow velocities and angles of attack.

8.1 Preliminary tests

Preliminary test was started with testing of all sensor signals and carefully heating of SMA wires. The first measurement showed that deflection of trailing edge corresponds to modelling result and measurement result achieved with smaller scale test specimen. After some measurement cycles deflection of trailing edge sharply decreased. The most probably reason for that is that the bonding between matrix and SMA wires was loosen and R-phase transformation (limited to 0.7%) is not any more able to deflect laminate as much as in the beginning of testing. The second reason for this behaviour could be that some mistakes happened in the manufacturing process and SMA wires are not undergoing R-phase transformation but traditional martensite-austenite transformation. However this is unlikely because of achieved strain levels were remained in same level in the rest of tests and gradual functional fatigue typical for martensite-austenite transformation is not observed.

The results of preliminary testing are shown in *Fig. 31* and *Fig. 32*. In *Fig. 31* strain generation is shown as a function of temperature. The strain (positive elongation) of the low skin laminate start to saturate when temperature approach 65°C but strain (compression) of upper skin laminate still increases. However temperature is limited around 65°C because Tg temperature of laminate epoxy is close to 80°C. Exceeding of Tg could cause serious damage to structure.

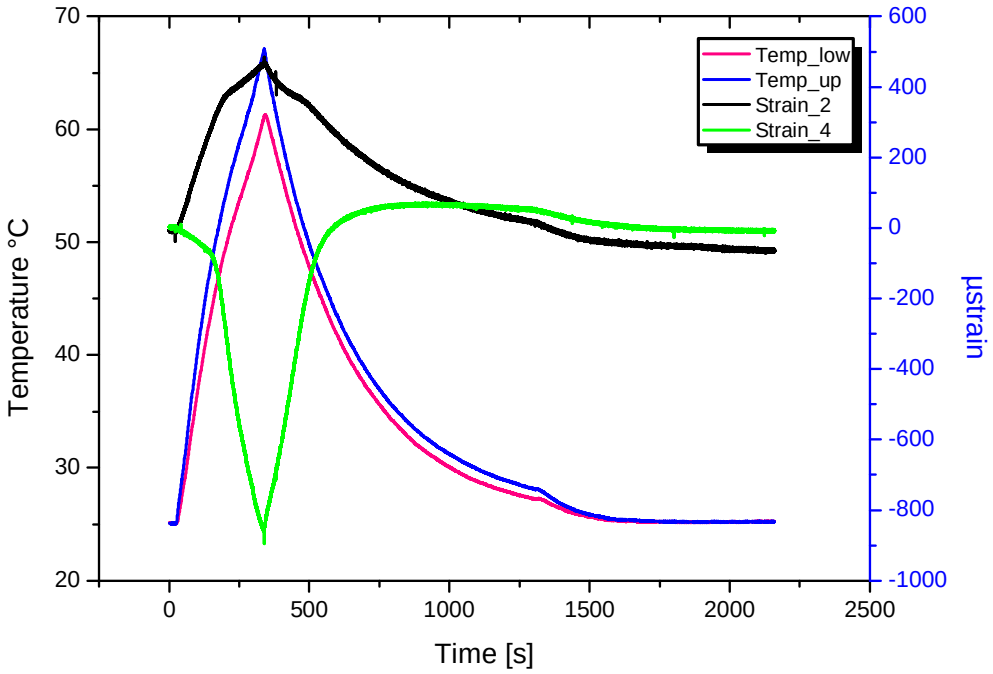

Fig. 31. Preliminary measurement of R-phase actuated trailing edge. Strain of the skin laminates as function of temperature (Strain_4 upper laminate and Strain_2 lower laminate).

In *Fig. 32*. shape change of trailing edge are shown corresponding strain measurement at peak temperatures. The maximum deflection of trailing edge is approximately 5 mm and change of angle correspondingly 5° at 100 mm distance from trailing edge.

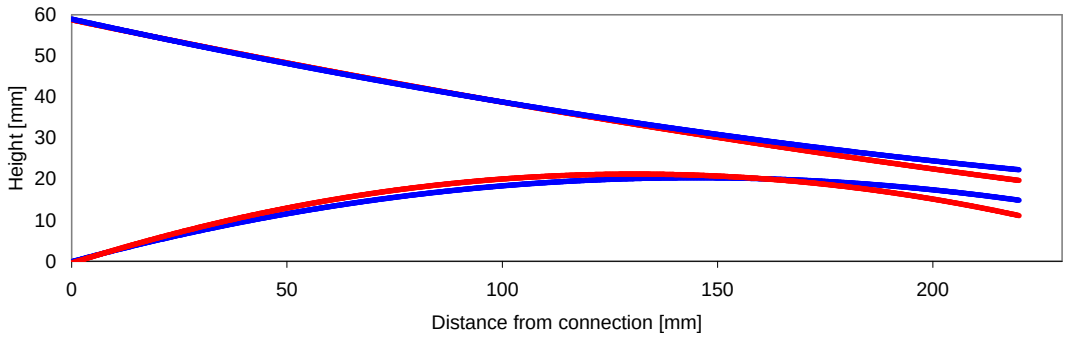

Fig. 32. Shape change of adaptive trailing edge: blue original shape and respectively red heat up to 60°.

8.2 Wind tunnel tests

Wind tunnel test were conducted in VTT icing wind tunnel. Because the tunnel is originally instrumented only for icing studies there is no possibility to measure lift and drag forces. The original idea was to scan shape of the airfoil and further calculate lift and drag by modelling, because achieved shape changes were limited remarkably smaller values than designed the test were limited only for the measurements of strains as function of temperature.

The original measurement plan was to heat up the adaptive trailing edge up to 65° and vary air flow speed and angle of attack. In preliminary test runs, the cooling effect of air flow was detected higher than expected which leads situation where maximum temperature were limited due to capacity of power amplifier. Because of tight measurement schedule it was agreed to accept the situation and conduct a modified test route with limited maximum activation temperature. The test setup is shown in *Fig. 33*.

.

Fig. 33. Wind tunnel test setup.

The test series consist of three wind speeds 20, 30 and 40 m/s. The effect of attack angle was studied with wind speed of 20 m/s by varying angle 0°, 4°, 8° and 12°. Zero angle was determined as centre line of the airfoil. With higher wind speed 30 m/s and 40 m/s only angle of attack 12° was studied.

In *Fig. 34* a)-d) effect of angle of attack on behaviour of adaptive trailing edge was shown. It should be noticed that due to problems with power source maximum achieved temperature is slightly varied. With higher angle of attacks 8° and 12° the activation temperature is approximately 5°C higher than smaller angles 0° and 4°. The highest strain levels were achieved with 12° angle of attack when strain values on both sides are close to 550 µstrain corresponding 0.55% strain.

The effect of wind speed is shown in *Fig. 34* d) and *Fig. 35* a)-b)

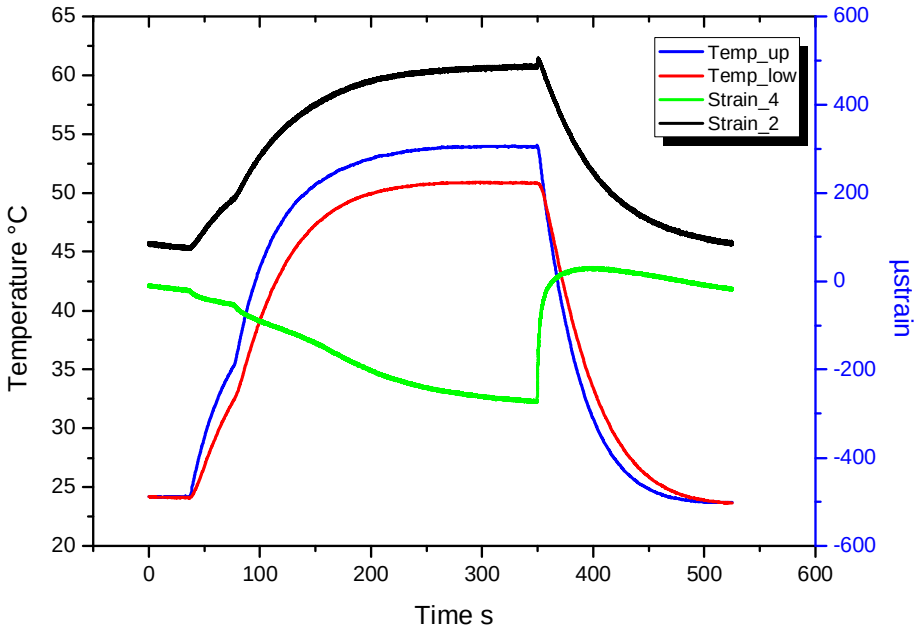

a) Angle of attack 0°, wind speed 20 m/s

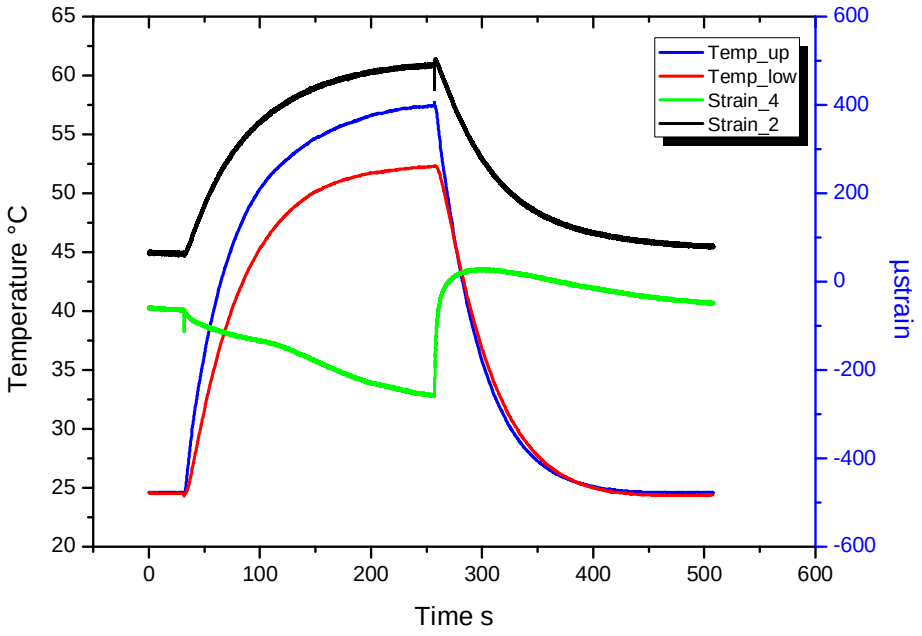

b) Angle of attack 4°, wind speed 20 m/s

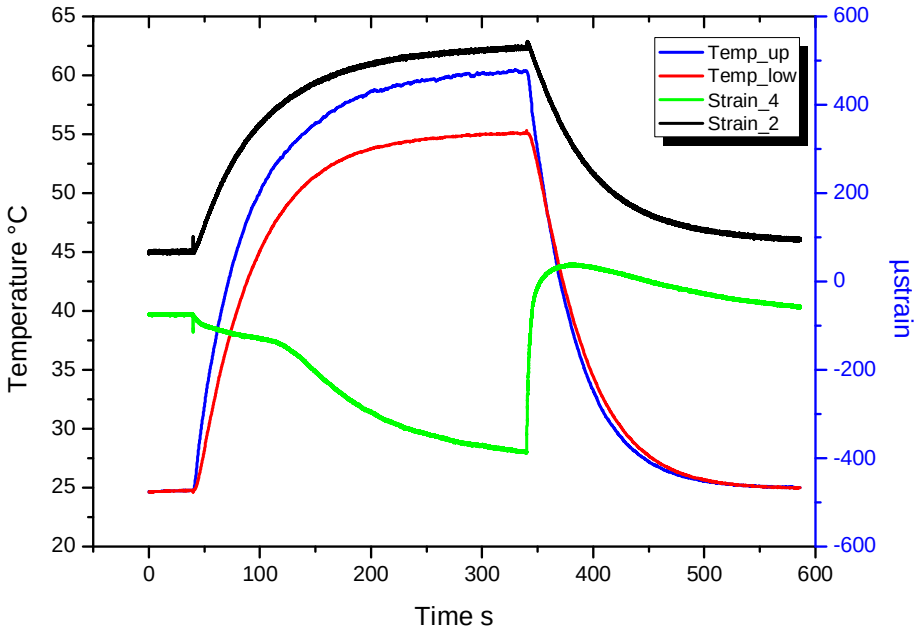

c) Angle of attack 8°, wind speed 20 m/s

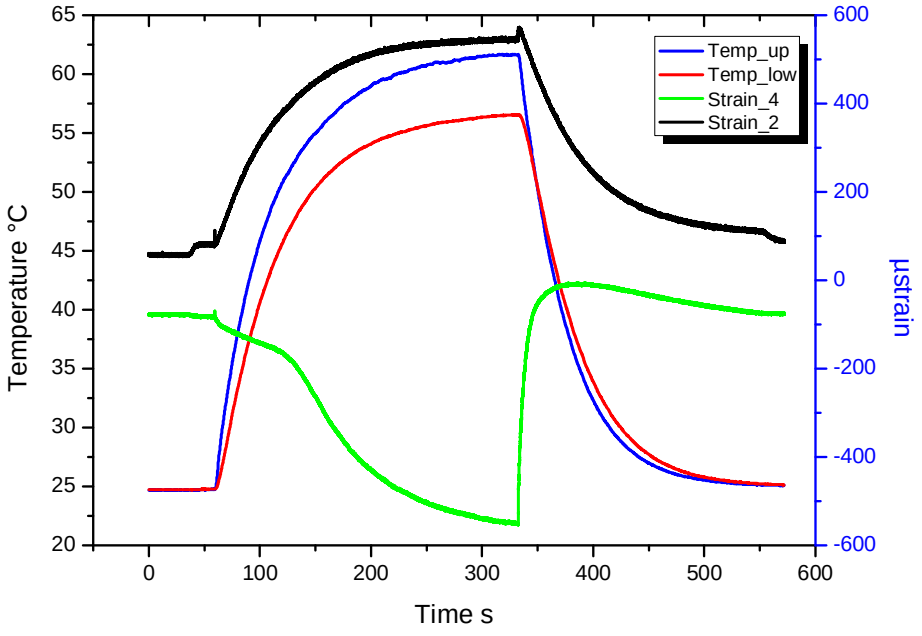

d) Angle of attack 12°, wind speed 20 m/s

Fig. 34. Behaviour of adaptive trailing edge at different angle of attacks a)-d) with wind speed 20 m/s.

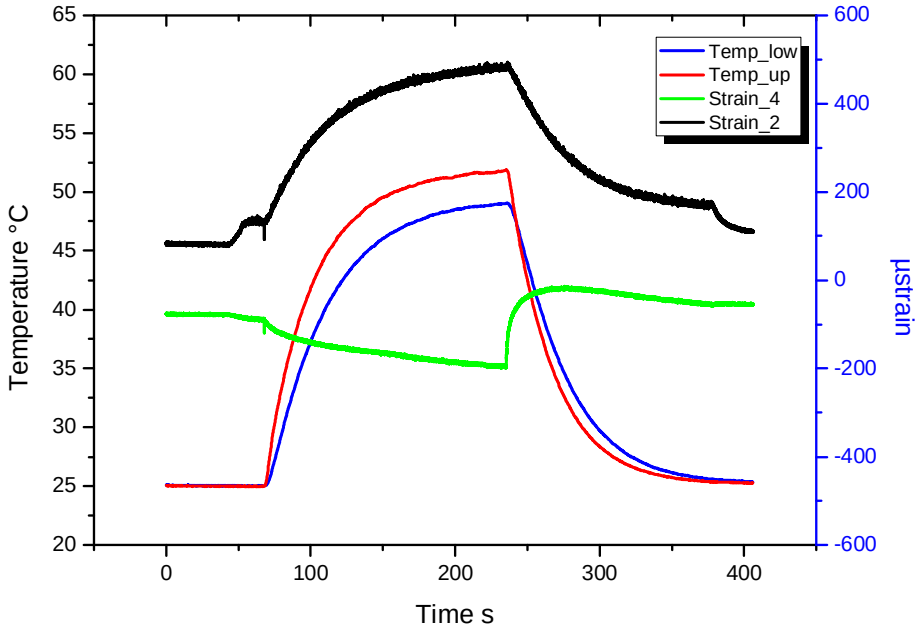

a) Angle of attack 12°, wind speed 30 m/s

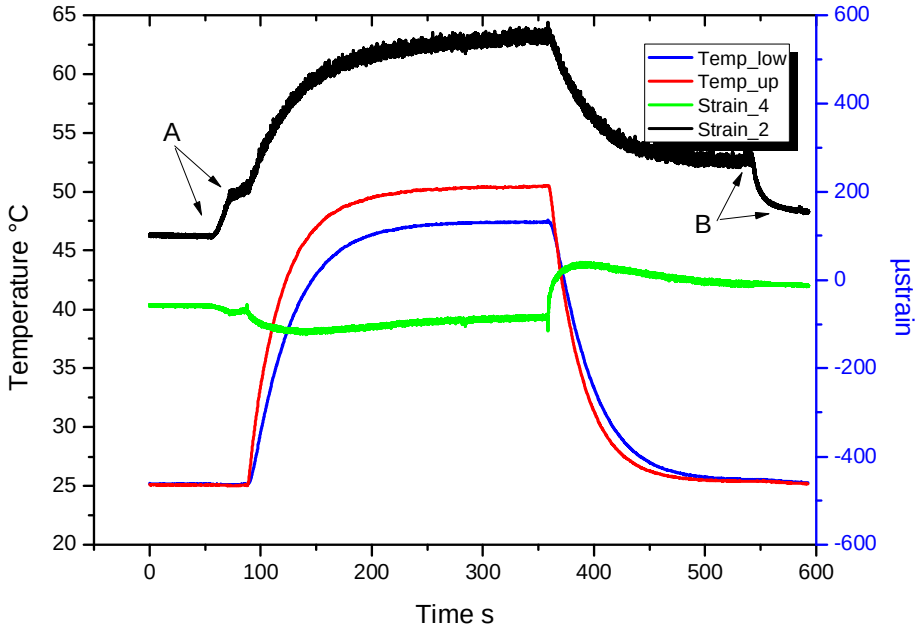

b) Angle of attack 12°, wind speed 40 m/s. Deflection due to wind speed is marked as A and B.

Fig. 35. Effect of wind speed on behaviour of adaptive trailing edge.

Effect of wind speed was measured so that also the deflection without activation related to wind speed could be determined. Strain measurement was started and after that wind tunnel fan is started with same manner wind tunnel fan is firstly stopped and stain measurement stopped when air flow was zero. In *Fig. 34* d) and *Fig. 35* a)-b) small steps at the beginning and the end of measured strain curve (especially Strain_2) can be observed corresponding to deflection due to wind speed. In *Fig. 35* b) these step are shown as A and B. As expected initial stain due to wind speed increases as function of wind speed from value 0.02% to 0.1%.

To get more easily comparable data, the strain levels at 50°C were collected (*Fig. 36* and *Fig. 37*). It can be noticed that angle of attack has only minor effect to the achieved strain level at 20 m/s wind speed. In the case of effect of wind speed, larger differences can be detected. Values of Strain 2 are gradually increasing as a function of wind speed. Strain 4 values are remaining at the same level with wind speed 30 m/s than detected in 20 m/s, but with wind speed 40 m/s the value drops remarkably. The conclusion is that forces created by wind speed 40 m/s at 12° angle of attack are higher than SMA actuators can produce.

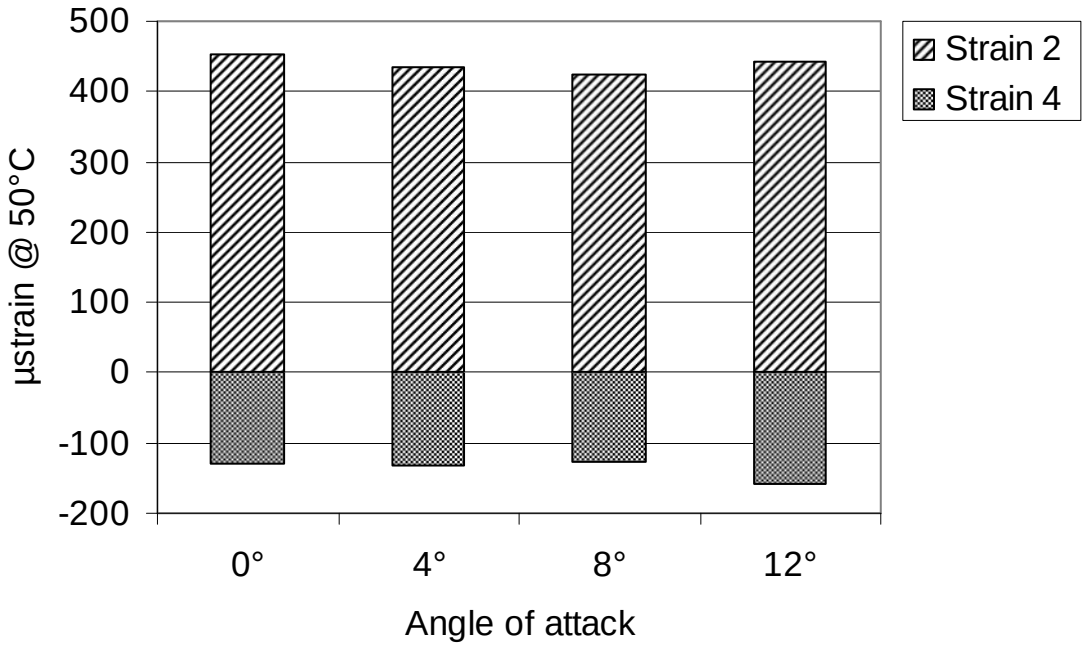

Fig. 36. Effect of angle of attack on achieved strain level at 50°C activation temperature (Strain 4 upper skin laminate and Strain 2 lower skin laminate).

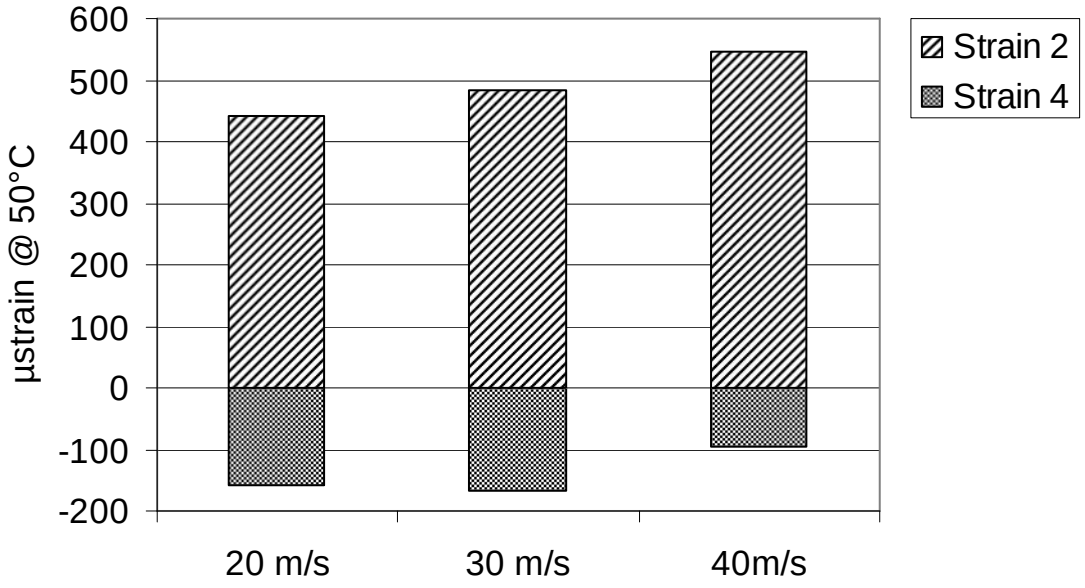

Fig. 37. Effect of wind speed to achieved strain level at 50°C activation temperature with angle of attack 12°.

9. Conclusions

Modelling and manufacturing tools for designing and producing of SMA actuated composites were developed. Prototype based on conventional SMA martensite-austenite transformation was designed, manufactured and tested in wind tunnel.

Wind tunnel tests show that lift force can be approximately doubled by activation of embedded SMA wires. Because of relatively high hysteresis of martensite-austenite transformation and poor heat conductivity of polymer composite, the operational frequency of adaptive airfoil is rather limited. This means that this type of adaptive airfoil can be used only for reacting against rather slow pacing phenomena.

To achieve higher operating frequency and higher resistance against functional fatigue, a manufacturing route for SMA composite based on R-phase transformation was developed. To meet concerns towards reliability and maintenance of adaptive blade structure, a novel modular design for adaptive trailing edge was introduced. The design is easily adapted for different kind of actuator and sensor concepts.

EMFi sensor network was preliminary tested for online detection for disturbance of air flow at the surface of airfoil. The concept looks promising for further development as sensory methodology for adaptive structures.

R-phase actuated airfoil was tested in wind tunnel. The achieved shape changes were smaller than expected, most probably due to some unfortunate damage during the preliminary testing. Overall wind tunnel tests were shown that adaptive structure works as planned. Only with the highest wind speed 40 m/s and 12° angle of attack, a remarkable deflection of structure due to wind speed was observed and deflection caused the R-phase transformation to be partially suppressed. The maximum operat-

ing frequency achievable with embedded R-phase actuated SMA wire was detected to be close 1 Hz. Operating frequency is mainly limited by heat conductivity of polymer matrix.

Utilization of R-phase transformation looks the most potential concept when SMA actuated composites are considered. Despite of this, there is still a lot of work to do with more simple and more reliable manufacturing route. One should notice that operating frequency is still limiting factor in many cases.

10. References

[i] Troldborg N.: Computational study of the Risoe B1-18 airfoil with a hinged flap providing variable trailing edge geometry, Wind Engineering, Vol 29, No 2, 2005, pp. 89-113

[ii] Z.G. Wei, R. Sandström, S. Miyazaki . J. Mater. Sci. 33 (1998) 3741-3762

[iii] Z.G. Wei, R. Sandström, S. Miyazaki . J. Mater. Sci. 33 (1998) 3763-3783

[iv] T.L.Turner, C. L. Lach, R. J. Cano, SPIE Vol. 4333, Paper No. 4333-60

[v] Y. Xu, K. Otsuka, H. Yoshida, H.Nagai, R. Oishi, H. Horikawa, T. Kishi, Intermetallics 10 (2000) 361-369

[vi] K. Lau, W. Tam, X. Meng, L. Zhou, Materials Letters 57 (2002) 364-368

[vii] Stanewsky E.: Adaptive wing and flow control technology, Progress in Aerospace sciences, Vol 37, No 7, 2001, pp. 583-667

[viii] Bein Th., Hanselka H., Breitbach E.: An adaptive spoiler to control the transonic shock, Smart Materials and Structures, Vol 9, 2000, pp. 141-148

[ix] Tsoi K.A., Schrooten J., Zheng Y., Stalmans R.: Part II. Thermomechanical characteristics of shape memory alloy composites, Mater. Sci. Eng. A, Vol 368, 2004, No 1-2, pp 299-310.

[x] Stalmans R., Tsoi K., Schrooten J.: The transformational behaviour of shape memory wires embedded in a composite matrix, Fifth European Conference on Smart Structures and Materials, Glasgow, Scotland, May 22-24, 2000, P.F. Gobin, C.M. Friend (Eds.), Proceedings of SPIE, Vol. 4073, pp. 88-96, 2000.

[xi] Jonnalagadda K.D., Sottos N.R., Qidwai M.A. and Lagoudas D.C.: In situ displacement measurements and numerical predictions of embedded SMA transformation, Smart Materials and Structures, Vol 9, 2000, pp. 701-710

[xii] Lauri Kantola, Tuomo Jokisalo, Tomi Lindroos. Sebastian Segercrantz, Timo Brander. Merja Sippola & Kalervo Nevala, CONTROLLING THE SHAPE OF A WING PROFILE UTILIZING

EMBEDDED SHAPE MEMORY ALLOY ACTUATORS AND DIFFERENT SENSORS, Smart Systems 2006 & ICMA 2006 , Seinäjoki